Journal of Computational Physics 372 (2018) 748–772

Contents lists available at ScienceDirect

Journal of Computational Physics

www.elsevier.com/locate/jcp

# A high-order perturbation of surfaces method for vector electromagnetic scattering by doubly layered periodic crossed gratings

Youngjoon Hong, David P. Nicholls *

*Department of Mathematics, Statistics, and Computer Science, University of Illinois at Chicago, Chicago, IL, 60607 USA*

ARTICLE INFO

*Article history:*
Received 15 March 2018
Received in revised form 11 June 2018
Accepted 12 June 2018
Available online xxxx

*Keywords:*
High-order spectral methods
Vector electromagnetic scattering
Periodic doubly layered media
High-order perturbation of surfaces methods

ABSTRACT

The accurate simulation of scattering of electromagnetic waves in three dimensions by a diffraction grating is crucial in many applications of engineering and scientific interest. In this contribution we present a novel High-Order Perturbation of Surfaces method for the numerical approximation of vector electromagnetic scattering by a doubly periodic layered medium. For this we restate the governing time harmonic Maxwell equations as vector Helmholtz equations which are coupled by transmission boundary conditions at the layer interface. We then apply the method of Transformed Field Expansions which delivers a Fourier collocation, Legendre–Galerkin, Boundary Perturbation approach to solve the problem in transformed coordinates. A sequence of numerical simulations demonstrate the efficient and robust spectral convergence which can be achieved with the proposed algorithm.



## 1. Introduction

The accurate simulation of scattering of electromagnetic waves in three dimensions by a diffraction grating is crucial in many applications of engineering and scientific interest. Examples include surface enhanced Raman scattering [72], extraordinary optical transmission [28], surface enhanced spectroscopy [50], photovoltaic devices [1], and surface plasmon resonance biosensing [38,47]. Clearly, the ability to numerically simulate such configurations with speed, accuracy, and robustness is of the utmost importance to many disciplines. In this contribution we present a novel High-Order Perturbation of Surfaces (HOPS) method for the numerical approximation of vector electromagnetic scattering by a periodic doubly layered medium.

Volumetric approaches to these problems are pervasive in the engineering literature. More specifically Finite Difference [46], Finite Element [42], Discontinuous Galerkin [40], Spectral Element [27], and Spectral [32,71] methods are all widely used by practitioners. However, such methods are clearly disadvantaged with an unnecessarily large number of unknowns for the piecewise homogeneous problems we consider here. In addition, the faithful enforcement of outgoing wave conditions is problematic for these approaches typically necessitating approximations such as the Perfectly Matched Layer [4,5] or exact, non-reflecting boundary conditions [41,39,44,30,54,12] which spoil the sparseness properties of the relevant linear systems.

* Corresponding author.
*E-mail addresses:* hongy@uic.edu (Y. Hong), davidn@uic.edu (D.P. Nicholls).

https://doi.org/10.1016/j.jcp.2018.06.041
0021-9991/

For these reasons, surface methods are an ideal choice as they are orders of magnitude faster when compared to volumetric approaches due to the greatly reduced number of degrees of freedom required to resolve a computation. In addition, far-field boundary conditions are enforced exactly through the choice of the Green function. Consequently, these methods are a very appealing alternative which are gaining favor with practitioners. The most prevalent among these interfacial algorithms are those based upon Boundary Integral Equations (BIEs) [24,69], but these face difficulties. Most have been resolved in recent years through (i.) the use of sophisticated quadrature rules to deliver High-Order Spectral (HOS) accuracy; (ii.) the design of preconditioned iterative solvers with suitable acceleration [33]; (iii) new strategies to accelerate the convergence of the periodized Green function [13,11] (or avoiding its periodization entirely [9,22]); and (iv.) new approaches to deal with the Rayleigh singularities (widely known in the literature as "Wood's anomalies") [3,7,21]. As a result they are a compelling alternative for many problems of applied interest, however, two properties render them disadvantaged for the *parameterized* problems we consider as compared with the methods we advocate here: (i.) For geometries specified by the real value, $\varepsilon$, (here the deviation of the interface shapes from trivial), a BIE solver will provide a solution for a single value of $\varepsilon$. If this is changed then the solver must be initiated again; (ii.) the dense, non-symmetric positive definite systems of linear equations that must be solved with each simulation. As specific examples where such considerations arise, we point the interested reader to the work of the second author, F. Reitich, T. Johnson, and S.-H. Oh. on (i.) simulating "reflectivity maps" associated to multilayer plasmonic devices [61] and (ii.) determining the minimal configuration required to excite surface plasmons with shallow gratings [55]. In the former, the parameterized nature of the configuration and the associated reflectivity map would require a BIE to be restarted with each new data point (unlike the scheme we advocate here). In the latter, the geometry shape was, by design, a *very* small perturbation of a flat-interface configuration. For a BIE method the cost of simulating this is the same as that of approximating a grating with a large deformation, while a perturbative algorithm (such as the one we discuss in this paper) can run much more quickly.

In contrast, a High-Order Perturbation of Surfaces (HOPS) methodology effectively addresses these concerns. These formulations have the advantageous properties of BIE formulations (e.g., surface formulation, reduced numbers of degrees of freedom, and exact enforcement of far-field boundary conditions) while being immune to the shortcomings listed above: (i.) Since HOPS approaches are built upon expansions in the deformation parameter, $\varepsilon$, once the Taylor coefficients are known for the problem unknowns, one simply sums these for any choice of $\varepsilon$ to recover the solution rather than beginning a new simulation; (ii.) the perturbative nature of the scheme is built upon the flat-interface solution which is trivially solved in Fourier space by inverting a sparse operator at each wavenumber. We point out that the initial smallness assumption on the deformation parameter, $\varepsilon$, can be dropped in light of the analytic continuation results in [58,34] which demonstrate that the domain of analyticity contains a neighborhood of the *entire* real axis. Therefore, with appropriate numerical analytic continuation methodologies (e.g., Padé approximation [10]) to access this region of analyticity, quite large and irregular perturbations can be simulated. We direct the interested reader to [15,17,20,57,60] for numerical demonstrations.

There are several approaches to HOPS simulation of partial differential equations posed on irregular domains, but they all trace their beginnings to low-order calculations such as those of Rayleigh [67] and Rice [68]. The first high-order incarnations appeared in the early 1990s with the introduction of the methods of Operator Expansions (OE) by Milder [48,49,51,52] and Field Expansions (FE) by Bruno and Reitich [14–16]. Each has been enhanced by various authors, but the most significant was the stabilization of these methods by one of the authors and Reitich with the Transformed Field Expansions (TFE) algorithm [56–60]. Beyond this, these HOPS schemes have been extended in a number of directions. Of particular interest to this contribution we mention bounded obstacle configurations [19,62,29], the full vector Maxwell equations [18,53,64] and a rigorous numerical analysis [63].

In addition to these, the authors have initiated a comprehensive study of the TFE recursions for linear wave scattering and their extension to multiple (three) layers in two dimensions [36] and multiple (arbitrary numbers of) layers in three dimensions [35]. However, these investigations fixed upon the scalar Helmholtz equations which only govern electromagnetic wave propagation in two dimensions under Transverse Electric or Transverse Magnetic polarization [65]. In this contribution we examine the much more difficult problem of simulating electromagnetic radiation scattered by a crossed grating in three dimensions in general polarization. This demands that we not only solve the vector Helmholtz equations in three dimensions, but also accommodate the more subtle interfacial boundary conditions of continuity of tangential fields with appropriate jumps in the normal direction. To this one must also add divergence-free constraints while imposing appropriate outgoing wave conditions to avoid pollution of solutions. We demonstrate how this can be achieved in the doubly layered scenario for which the TFE recursions have yet to be derived and implemented. Of particular note, we describe a novel, spectrally accurate, modified Legendre–Galerkin approach to the vertical discretization where the standard basis is enriched with additional connecting basis functions across the layer boundary.

In addition to the novelty of our new algorithm for this model, we also point out that our approach will be the method of choice for simulating the technologically relevant case of homogeneous layers separated by an interface which is a slight to moderate deviation of flat. In this case volumetric approaches will not be competitive due to their onerous operation counts and memory requirements, while BIE approaches (which have the same memory constraints as our TFE method) will take longer as their computational cost in this setting will be significantly greater. The combination of (i.) dense, non-symmetric positive-definite matrix inversion, and (ii.) the algorithmic and operational complications of evaluating the Green function (both its periodization and accounting for the Rayleigh singularities) render such approaches non-competitive for the problems we consider here.

The article is organized as follows: In Section 2 the governing equations for linear electromagnetic waves interacting with a periodic doubly layered structure are carefully formulated, together with the appropriate interfacial boundary conditions. The TFE method is described in Section 3, and the modified Legendre–Galerkin scheme, which we implemented for the vertical discretization, is discussed in Sections 4 and 5. A sequence of numerical experiments are presented in Section 6 which demonstrate the stability and accuracy we can achieve in simulations of configurations containing not only smooth and small interfaces, but also rough and large ones as well.

## 2. Governing equations

In this section we describe the governing equations of linear electromagnetic waves scattered by a doubly layered medium. Consider a grating structure with crossed periodic interface located at

$$z = g(x, y), \quad g(x + d_1, y + d_2) = g(x, y),$$

where $z$ is the vertical coordinate, and $x$ and $y$ are the lateral coordinates. Dielectrics occupy each of the two domains

$$S_g^1 := \{z > g(x, y)\}, \quad S_g^2 := \{z < g(x, y)\},$$

with constant permittivities and permeabilities, $\{\epsilon_m, \mu_m\}$ $(m = 1, 2)$, in each of the layers. The structure is illuminated from above by time-harmonic (with frequency $\omega$) plane-wave incidence of the (reduced) form

$$\mathbf{H}^{\text{inc}} = \mathbf{A}e^{i(\alpha x+\beta y-\gamma z)}, \qquad \nabla \cdot \mathbf{H}^{\text{inc}} = 0, \tag{1a}$$

$$\mathbf{E}^{\text{inc}} = \mathbf{B}e^{i(\alpha x+\beta y-\gamma z)}, \qquad \nabla \cdot \mathbf{E}^{\text{inc}} = 0, \tag{1b}$$

where

$$\mathbf{A} \cdot (\alpha, \beta, -\gamma)^T = 0, \quad \mathbf{B} = -\frac{1}{i\omega\epsilon_1}\nabla \times \mathbf{A}.$$

We follow the convention that bold-faced characters denote vectors and plain-faced are scalars, so that, for instance, $\mathbf{A} = (A^x, A^y, A^z)^T$.

In this setting electromagnetic radiation is governed by the time-harmonic forms of Faraday's and Ampere's Laws

$$\nabla \times \mathbf{E} - i\omega\mu\mathbf{H} = 0, \tag{2a}$$

$$\nabla \times \mathbf{H} + i\omega\epsilon\mathbf{E} = 0, \tag{2b}$$

respectively, which govern the reduced electric, $\mathbf{E}$, and magnetic, $\mathbf{H}$, fields. We consider $\mu = \mu_0$, the permeability of the vacuum, and the permittivity a piecewise constant

$$\epsilon = \begin{cases} \epsilon_1, & \text{in } S_g^1, \\ \epsilon_2, & \text{in } S_g^2. \end{cases}$$

As there are no sources (current or charge), applying the divergence operator to (2) and using the fact that the divergence of a curl is zero, reveals Gauss' Law for Magnetism and Gauss' Law

$$\text{div}\,[\mu_0\mathbf{H}] = 0, \quad \text{div}\,[\epsilon\mathbf{E}] = 0, \tag{3}$$

respectively, inside each layer. By applying the curl operator to (2) and using (3) one can see that each field satisfies the vector Helmholtz equations

$$\Delta\mathbf{E} + k^2\mathbf{E} = 0, \quad \Delta\mathbf{H} + k^2\mathbf{H} = 0, \tag{4}$$

where $k^2 = \omega^2\epsilon\mu$. We decompose the total magnetic and electric fields into reflected (layer 1) and transmitted (layer 2) components in the following way

$$\mathbf{E} = \begin{cases} \mathbf{E}_1 + \mathbf{E}^{\text{inc}}, & \text{in } S_g^1, \\ \mathbf{E}_2, & \text{in } S_g^2, \end{cases} \quad \mathbf{H} = \begin{cases} \mathbf{H}_1 + \mathbf{H}^{\text{inc}}, & \text{in } S_g^1, \\ \mathbf{H}_2, & \text{in } S_g^2, \end{cases}$$

and note that each of the $\{\mathbf{E}_m, \mathbf{H}_m\}$ also satisfy the vector Helmholtz equations, (4).

At this point we remark that it is sufficient to solve for the magnetic fields, $\mathbf{H}_m$, as the electric fields, $\mathbf{E}_m$, can be recovered from (2b),

$$\mathbf{E}_m = -\frac{1}{i\omega\epsilon_m}\nabla \times \mathbf{H}_m.$$

We could, of course, select the electric field as our unknown and recover the magnetic field from (2a). However, as we shall see, the magnetic field enjoys better smoothness properties across the grating interface (its normal component is continuous) than the electric field.

With this choice we select (4) as the governing equations for our unknowns $\mathbf{H}_m$ in the bulk and now must specify boundary conditions for these. First, the periodicity of the grating interface demands quasiperiodicity of the fields, [65],

$$\mathbf{H}_m(x+d_1, y+d_2, z) = e^{i\alpha d_1 + i\beta d_2}\mathbf{H}_m(x, y, z).$$

Additionally, the scattered fields must be "outgoing" (upward propagating in $S_g^1$ and downward propagating in $S_g^2$) which we make precise in Section 2.1.

For interfacial boundary conditions, an application of Stokes' Theorem to (2a) and (2b) yields the continuity of *tangential* components of the electric and magnetic fields in the absence of interface sources (currents and charges)

$$\mathbf{N} \times \left(\mathbf{E}_1 + \mathbf{E}^{\text{inc}} - \mathbf{E}_2\right) = 0, \qquad \text{at } \Gamma, \tag{5a}$$

$$\mathbf{N} \times \left(\mathbf{H}_1 + \mathbf{H}^{\text{inc}} - \mathbf{H}_2\right) = 0, \qquad \text{at } \Gamma, \tag{5b}$$

where $\mathbf{N} = (-\partial_x g, -\partial_y g, 1)^T$ is an upward pointing normal and $\Gamma$ denotes the interface

$$\Gamma := \{(x, y, z) \mid z = g(x, y)\}.$$

Using (2b), the first of these, (5a), can be written in terms of the magnetic field as

$$\mathbf{N} \times \left(\nabla \times \mathbf{H}_1 + \nabla \times \mathbf{H}^{\text{inc}} - \tau \nabla \times \mathbf{H}_2\right) = 0, \quad \text{at } \Gamma, \tag{6}$$

where

$$\tau := \frac{\epsilon_1}{\epsilon_2} = \frac{k_1^2}{k_2^2}.$$

The divergence theorem applied to (3) delivers the jump relations in the *normal* components of the fields

$$\mathbf{N} \cdot \left(\epsilon_1 \mathbf{E}_1 + \epsilon_1 \mathbf{E}^{\text{inc}} - \epsilon_2 \mathbf{E}_2\right) = 0, \qquad \text{at } \Gamma, \tag{7a}$$

$$\mathbf{N} \cdot \left(\mathbf{H}_1 + \mathbf{H}^{\text{inc}} - \mathbf{H}_2\right) = 0, \qquad \text{at } \Gamma, \tag{7b}$$

where we have used $\mu = \mu_0$ to simplify the latter. From these we discover that the change in permittivity across $\Gamma$ induces a jump in the normal component of the electric field, while the constant value of the permeability yields a magnetic field with continuous normal component.

However, as noted in [23], there is redundancy in these conditions so we appeal to the work of [45,43] who demonstrate that for a sufficiently regular interface (Lipschitz continuous is smooth enough) the divergence free conditions in the bulk, (3), can be guaranteed by simply enforcing them at the interface

$$\text{div}\,[\epsilon_m \mathbf{E}_m] = 0, \quad \text{div}\,[\mathbf{H}_m] = 0, \quad \text{at } \Gamma. \tag{8}$$

We have now presented eight interfacial boundary conditions, but six should suffice for the six unknowns in (4). For our developments we find it most convenient to select (5b), (6), (7b), and the *difference* of the latter equation in (8) between $\mathbf{H}_1$ and $\mathbf{H}_2$.

Gathering all of these equations, we now focus on the following problem

$$\Delta \mathbf{H}_1 + k_1^2 \mathbf{H}_1 = 0, \qquad \text{in } S_g^1, \tag{9a}$$

$$\Delta \mathbf{H}_2 + k_2^2 \mathbf{H}_2 = 0, \qquad \text{in } S_g^2, \tag{9b}$$

$$\mathbf{N} \times (\mathbf{H}_1 - \mathbf{H}_2) = -\mathbf{N} \times \mathbf{H}^{\text{inc}}, \qquad \text{at } \Gamma, \tag{9c}$$

$$\mathbf{N} \cdot (\mathbf{H}_1 - \mathbf{H}_2) = -\mathbf{N} \cdot \mathbf{H}^{\text{inc}}, \qquad \text{at } \Gamma, \tag{9d}$$

$$\mathbf{N} \times (\nabla \times \mathbf{H}_1 - \tau \nabla \times \mathbf{H}_2) = -\mathbf{N} \times \nabla \times \mathbf{H}^{\text{inc}}, \qquad \text{at } \Gamma, \tag{9e}$$

$$\text{div}\,[\mathbf{H}_1] - \text{div}\,[\mathbf{H}_2] = 0, \qquad \text{at } \Gamma, \tag{9f}$$

$$\text{OWC}[\mathbf{H}_1] = 0, \qquad z \to \infty, \tag{9g}$$

$$\text{OWC}[\mathbf{H}_2] = 0, \qquad z \to -\infty, \tag{9h}$$

where "OWC" stands for the outgoing (upward/downward propagating) wave condition which we make precise presently [2].

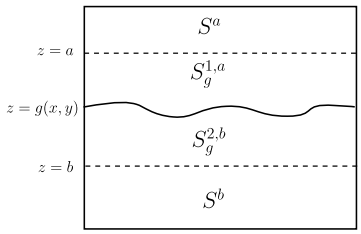


**Fig. 1.** A depiction of the layered grating structure with artificial boundaries at $z = a$ and $z = b$.

**Remark 1.** An inspection of the mathematically careful literature shows that while our formulation is largely standard, the appearance of two of our surface conditions, (9d) and (9f), while true, are somewhat unusual. However, a more careful reading of these papers typically reveals that the bulk divergence-free conditions (3), or their surface versions (8), are used in rather subtle and implicit ways at important points of the analysis. One of our goals in this work is to make all of this *explicit* in the problem statement with a view towards efficient and high-order numerical simulation (rather than rigorous analysis). Our choice was one of many we could have made, and it was simply the one most convenient for our implementation.

### 2.1. Transparent boundary conditions

The usual procedure when implementing the TFE method is to truncate the unbounded problem domain to a bounded one using a transparent (non-reflecting) boundary condition. For this we introduce artificial boundaries above and below the structure, and enforce boundary conditions to solve (9) equivalently. Introducing the planes

$$z = a > |g|_{L^\infty}, \qquad z = b < -|g|_{L^\infty},$$

we define the domains

$$S^a := \{z > a\}, \quad S^b := \{z < b\},$$
$$S_g^{1,a} := \{g(x, y) < z < a\}, \quad S_g^{2,b} := \{b < z < g(x, y)\};$$

see, e.g., Fig. 1. Transparent boundary conditions can be enforced with Dirichlet–Neumann Operators (DNOs) from the Rayleigh expansions [67] in the following way. More specifically, it is known [65] that

$$\mathbf{H}_1(x, y, z) = \sum_{p=-\infty}^{\infty} \sum_{q=-\infty}^{\infty} \hat{\mathbf{t}}_{p,q} e^{i(\alpha_p x + \beta_q y + \gamma_{p,q}^{(1)}(z-a))}, \quad z > a,$$

and

$$\mathbf{H}_2(x, y, z) = \sum_{p=-\infty}^{\infty} \sum_{q=-\infty}^{\infty} \hat{\mathbf{s}}_{p,q} e^{i(\alpha_p x + \beta_q y + \gamma_{p,q}^{(2)}(b-z))}, \quad z < b,$$

where, for $p, q \in \mathbf{Z}$,

$$\alpha_p := \alpha + (2\pi/d_1)p, \quad \beta_q := \beta + (2\pi/d_2)q,$$

and

$$\gamma_{p,q}^{(m)} := \begin{cases} \sqrt{k_m^2 - \alpha_p^2 - \beta_q^2}, & (p, q) \in \mathcal{U}^m, \\ i\sqrt{\alpha_p^2 + \beta_q^2 - k_m^2}, & (p, q) \notin \mathcal{U}^m, \end{cases} \quad m = 1, 2,$$

and the set of propagating modes is

$$\mathcal{U}^m := \{p, q \in \mathbf{Z} \mid \alpha_p^2 + \beta_q^2 < k_m^2\}, \quad m = 1, 2.$$

It is not difficult to see that these solutions satisfy the Dirichlet conditions

$$\mathbf{H}_1(x, y, a) = \sum_{p=-\infty}^{\infty} \sum_{q=-\infty}^{\infty} \hat{\mathbf{t}}_{p,q} e^{i(\alpha_p x + \beta_q y)} =: \mathbf{t}(x, y),$$

$$\mathbf{H}_2(x, y, b) = \sum_{p=-\infty}^{\infty} \sum_{q=-\infty}^{\infty} \hat{\mathbf{s}}_{p,q} e^{i(\alpha_p x + \beta_q y)} =: \mathbf{s}(x, y).$$

From these we can compute the Neumann data at the artificial boundaries,

$$\partial_z \mathbf{H}_1(x,y,a) = \sum_{p=-\infty}^{\infty}\sum_{q=-\infty}^{\infty} (i\gamma_{p,q}^{(1)})\hat{\mathbf{t}}_{p,q} e^{i(\alpha_p x+\beta_q y)},$$

$$\partial_z \mathbf{H}_2(x,y,b) = \sum_{p=-\infty}^{\infty}\sum_{q=-\infty}^{\infty} (-i\gamma_{p,q}^{(2)})\hat{\mathbf{s}}_{p,q} e^{i(\alpha_p x+\beta_q y)},$$

and thus we define the DNOs

$$T_1[\mathbf{t}] := \sum_{p=-\infty}^{\infty}\sum_{q=-\infty}^{\infty} (i\gamma_{p,q}^{(1)})\hat{\mathbf{t}}_{p,q} e^{i(\alpha_p x+\beta_q y)},$$

$$T_2[\mathbf{s}] := \sum_{p=-\infty}^{\infty}\sum_{q=-\infty}^{\infty} (-i\gamma_{p,q}^{(2)})\hat{\mathbf{s}}_{p,q} e^{i(\alpha_p x+\beta_q y)},$$

which are order-one Fourier multipliers.

Using these DNOs at the artificial boundaries we write (9) *equivalently* on the bounded domain $\{b < z < a\}$,

$$\Delta\mathbf{H}_1 + k_1^2\mathbf{H}_1 = 0, \qquad \text{in } S_g^{1,a}, \tag{10a}$$

$$\Delta\mathbf{H}_2 + k_2^2\mathbf{H}_2 = 0, \qquad \text{in } S_g^{2,b}, \tag{10b}$$

$$\mathbf{N}\times(\mathbf{H}_1-\mathbf{H}_2) = -\mathbf{N}\times\mathbf{H}^{\text{inc}}, \qquad \text{at } \Gamma, \tag{10c}$$

$$\mathbf{N}\cdot(\mathbf{H}_1-\mathbf{H}_2) = -\mathbf{N}\cdot\mathbf{H}^{\text{inc}}, \qquad \text{at } \Gamma, \tag{10d}$$

$$\mathbf{N}\times(\nabla\times\mathbf{H}_1 - \tau\nabla\times\mathbf{H}_2) = -\mathbf{N}\times\nabla\times\mathbf{H}^{\text{inc}}, \qquad \text{at } \Gamma, \tag{10e}$$

$$\text{div}\,[\mathbf{H}_1] - \text{div}\,[\mathbf{H}_2] = 0, \qquad \text{at } \Gamma, \tag{10f}$$

$$\partial_z\mathbf{H}_1 - T_1[\mathbf{H}_1] = 0, \qquad \text{at } z=a, \tag{10g}$$

$$\partial_z\mathbf{H}_2 - T_2[\mathbf{H}_2] = 0, \qquad \text{at } z=b, \tag{10h}$$

which are our governing equations.

## 3. Transformed field expansions

We are now in a position to describe our TFE method. As always, the algorithm begins with a domain flattening change of variables [56] (also known as $\sigma$-coordinates [66] in the geophysical literature and the C-method [25] in the electromagnetics community). Subsequently, a boundary perturbation expansion is conducted, resulting in a recurrently defined set of vector Helmholtz problems which must be solved at every perturbation order desired.

### 3.1. The change of variables

To begin we define the change of variables

$$x' = x, \quad y' = y,$$

$$z_1 = a\left(\frac{z-g}{a-g}\right), \qquad g < z < a, \quad a > |g|_{L^\infty},$$

$$z_2 = b\left(\frac{g-z}{g-b}\right), \qquad b < z < g, \quad b < -|g|_{L^\infty},$$

and the transformed fields

$$\mathbf{U}_m(x',y',z_m) := \mathbf{H}_m(x(x'),y(y'),z(x',y',z_m)), \quad m=1,2.$$

With this change of variables, a ponderous computation (see Appendix A) transforms (10) to the following system of equations

$$\Delta_1 \mathbf{U}_1 + k_1^2 \mathbf{U}_1 = \mathbf{R}_1, \qquad \text{in } 0 < z_1 < a, \tag{11a}$$

$$\Delta_2 \mathbf{U}_2 + k_2^2 \mathbf{U}_2 = \mathbf{R}_2, \qquad \text{in } b < z_2 < 0, \tag{11b}$$

$$[\![U^x]\!] = I_1, \qquad \text{at } z_1 = z_2 = 0, \tag{11c}$$

$$[\![U^y]\!] = I_2, \qquad \text{at } z_1 = z_2 = 0, \tag{11d}$$

$$[\![U^z]\!] = I_3, \qquad \text{at } z_1 = z_2 = 0, \tag{11e}$$

$$[\![\partial_{x'} U^z]\!]_\tau - [\![(G/C)\partial_z U^x]\!]_\tau = Q_1, \qquad \text{at } z_1 = z_2 = 0, \tag{11f}$$

$$[\![\partial_{y'} U^z]\!]_\tau - [\![(G/C)\partial_z U^y]\!]_\tau = Q_2, \qquad \text{at } z_1 = z_2 = 0, \tag{11g}$$

$$[\![\partial_{x'} U^x]\!] + [\![\partial_{y'} U^y]\!] + \frac{a}{a-g}\partial_z U_1^z - \frac{b}{b-g}\partial_z U_2^z = J, \qquad \text{at } z_1 = z_2 = 0, \tag{11h}$$

$$\partial_{z_1} \mathbf{U}_1 - T_1[\mathbf{U}_1] = \mathbf{B}_1, \qquad \text{at } z_1 = a, \tag{11i}$$

$$\partial_{z_2} \mathbf{U}_2 - T_2[\mathbf{U}_2] = \mathbf{B}_2, \qquad \text{at } z_2 = b, \tag{11j}$$

where

$$\mathbf{R}_m := \frac{1}{G_m^2}(\partial_{x'} R_m^x + \partial_{y'} R_m^y + \partial_{z_m} R_m^z + R_m^0), \quad m = 1, 2,$$

and

$$\begin{aligned}
I_1 &:= -\left((\partial_{x'} g) A^z + A^x\right) \varphi - (\partial_{x'} g)[\![U^z]\!], \\
I_2 &:= -\left((\partial_{y'} g) A^z + A^y\right) \varphi - (\partial_{y'} g)[\![U^z]\!], \\
I_3 &:= ((\partial_{x'} g) A^x + (\partial_{y'} g) A^y - A^z)\varphi + (\partial_{x'} g)[\![U^x]\!] + (\partial_{y'} g)[\![U^y]\!], \\
\varphi &:= e^{(i\alpha x + i\beta y - i\gamma g(x,y))},
\end{aligned}$$

and

$$\begin{aligned}
J &:= (\partial_{x'} g)\frac{a}{a-g}\partial_z U_1^x - (\partial_{x'} g)\frac{b}{b-g}\partial_z U_2^x + (\partial_{y'} g)\frac{a}{a-g}\partial_z U_1^y - (\partial_{y'} g)\frac{b}{b-g}\partial_z U_2^y, \\
\mathbf{B}_1 &:= -(g/a) T_1[\mathbf{U}_1], \\
\mathbf{B}_2 &:= -(g/b) T_2[\mathbf{U}_2],
\end{aligned}$$

and

$$[\![K]\!] := K_1 - K_2, \quad [\![K]\!]_\tau := K_1 - \tau K_2.$$

The Laplacian operator $\Delta_m$ is defined by

$$\Delta_m = \partial_{x'}^2 + \partial_{y'}^2 + \partial_{z_m}^2, \quad m = 1, 2.$$

We refer the reader to Appendix A for the specific formulas for the right hand sides $R_m^s$ and $Q_m$, (A.2) and (A.7), respectively.

### 3.2. A high-order perturbation of surfaces method

To specify our HOPS approach we consider an interface deformation of the form

$$g(x, y) = \varepsilon f(x, y), \quad \varepsilon \ll 1,$$

and insert this into the transformed equations (11). In a forthcoming publication it will be shown that the transformed fields depend *analytically* upon the parameter $\varepsilon$ so that the following expansions are valid

$$\mathbf{U}_m = \sum_{n=0}^{\infty} \mathbf{U}_{m,n}(x, y, z)\varepsilon^n, \quad m = 1, 2.$$

From (11) we find at each perturbation order that

$$\Delta_1 \mathbf{U}_{1,n} + k_1^2 \mathbf{U}_{1,n} = \mathbf{R}_{1,n}, \qquad \text{in } 0 < z_1 < a, \tag{12a}$$
$$\Delta_2 \mathbf{U}_{2,n} + k_2^2 \mathbf{U}_{2,n} = \mathbf{R}_{2,n}, \qquad \text{in } b < z_2 < 0, \tag{12b}$$
$$[\![ U_n^x ]\!] = I_{1,n}, \qquad \text{at } z_1 = z_2 = 0, \tag{12c}$$
$$[\![ U_n^y ]\!] = I_{2,n}, \qquad \text{at } z_1 = z_2 = 0, \tag{12d}$$
$$[\![ U_n^z ]\!] = I_{3,n}, \qquad \text{at } z_1 = z_2 = 0, \tag{12e}$$
$$[\![ \partial_{x'} U_n^z ]\!]_\tau - [\![ \partial_z U_n^x ]\!]_\tau = \widetilde{\mathrm{Q}}_{1,n}, \qquad \text{at } z_1 = z_2 = 0, \tag{12f}$$
$$[\![ \partial_{y'} U_n^z ]\!]_\tau - [\![ \partial_z U_n^y ]\!]_\tau = \widetilde{\mathrm{Q}}_{2,n}, \qquad \text{at } z_1 = z_2 = 0, \tag{12g}$$
$$[\![ \partial_{x'} U_n^x ]\!] + [\![ \partial_{y'} U_n^y ]\!] + [\![ \partial_z U_n^z ]\!] = \widetilde{J}_n, \qquad \text{at } z_1 = z_2 = 0, \tag{12h}$$
$$\partial_{z_1} \mathbf{U}_{1,n} - T_1[\mathbf{U}_{1,n}] = \mathbf{B}_{1,n}, \qquad \text{at } z_1 = a, \tag{12i}$$
$$\partial_{z_2} \mathbf{U}_{2,n} - T_2[\mathbf{U}_{2,n}] = \mathbf{B}_{2,n}, \qquad \text{at } z_2 = b. \tag{12j}$$

Again, we refer the reader to Appendix A for formulas for the right hand sides $\mathbf{R}_{m,n}$, $I_{s,n}$, $\widetilde{\mathrm{Q}}_{m,n}$, $\widetilde{J}_n$, and $\mathbf{B}_{m,n}$.

Considering the quasiperiodicity of solutions, we propose the following generalized Fourier (Floquet) series expansions

$$\{\mathbf{U}_{m,n}, \mathbf{R}_{m,n}\}(x,y,z) = \sum_{p=-\infty}^{\infty} \sum_{q=-\infty}^{\infty} \{\mathbf{U}_{m,n}^{p,q}, \mathbf{R}_{m,n}^{p,q}\}(z) e^{i(\alpha_p x + \beta_q y)},$$
$$\{I_{s,n}, \widetilde{\mathrm{Q}}_{m,n}, \widetilde{J}_n, \mathbf{B}_{m,n}\}(x,y) = \sum_{p=-\infty}^{\infty} \sum_{q=-\infty}^{\infty} \{I_{s,n}^{p,q}, \widetilde{\mathrm{Q}}_{m,n}^{p,q}, \widetilde{J}_n^{p,q}, \mathbf{B}_{m,n}^{p,q}\} e^{i(\alpha_p x + \beta_q y)}.$$

Inserting these expansions into (12), and using the fact that $(\gamma_{p,q}^{(m)})^2 = k_m^2 - \alpha_p^2 - \beta_q^2$, the governing equations are reduced to the one-dimensional boundary value problems

$$\partial_{z_1}^2 \mathbf{U}_{1,n}^{p,q} + (\gamma_{p,q}^{(1)})^2 \mathbf{U}_{1,n}^{p,q} = \mathbf{R}_{1,n}^{p,q}, \qquad \text{in } 0 < z_1 < a, \tag{13a}$$
$$\partial_{z_2}^2 \mathbf{U}_{2,n}^{p,q} + (\gamma_{p,q}^{(2)})^2 \mathbf{U}_{2,n}^{p,q} = \mathbf{R}_{2,n}^{p,q}, \qquad \text{in } b < z_2 < 0, \tag{13b}$$
$$[\![ U_n^{x,p,q} ]\!] = I_{1,n}^{p,q}, \qquad \text{at } z_1 = z_2 = 0, \tag{13c}$$
$$[\![ U_n^{y,p,q} ]\!] = I_{2,n}^{p,q}, \qquad \text{at } z_1 = z_2 = 0, \tag{13d}$$
$$[\![ U_n^{z,p,q} ]\!] = I_{3,n}^{p,q}, \qquad \text{at } z_1 = z_2 = 0, \tag{13e}$$
$$i\alpha_p [\![ U_n^{z,p,q} ]\!]_\tau - [\![ \partial_z U_n^{x,p,q} ]\!]_\tau = \widetilde{\mathrm{Q}}_{1,n}^{p,q}, \qquad \text{at } z_1 = z_2 = 0, \tag{13f}$$
$$i\beta_q [\![ U_n^{z,p,q} ]\!]_\tau - [\![ \partial_z U_n^{y,p,q} ]\!]_\tau = \widetilde{\mathrm{Q}}_{2,n}^{p,q}, \qquad \text{at } z_1 = z_2 = 0, \tag{13g}$$
$$i\alpha_p [\![ U_n^{x,p,q} ]\!] + i\beta_q [\![ U_n^{y,p,q} ]\!] + [\![ \partial_z U_{1,n}^{z,p,q} ]\!] = \widetilde{J}_n^{p,q}, \qquad \text{at } z_1 = z_2 = 0, \tag{13h}$$
$$\partial_{z_1} \mathbf{U}_{1,n}^{p,q} - i\gamma_{p,q}^{(1)} \mathbf{U}_{1,n}^{p,q} = \mathbf{B}_{1,n}^{p,q}, \qquad \text{at } z_1 = a, \tag{13i}$$
$$\partial_{z_2} \mathbf{U}_{2,n}^{p,q} + i\gamma_{p,q}^{(2)} \mathbf{U}_{2,n}^{p,q} = \mathbf{B}_{2,n}^{p,q}, \qquad \text{at } z_2 = b. \tag{13j}$$

We point out that the unique solvability of the full problem (9) [23,26,6] delivers a unique solution to (13).

## 4. Weak formulation

In this section, we construct a weak formulation of (13) by decomposing solutions into two parts

$$\mathbf{U}_{m,n}^{p,q} = \widetilde{\mathbf{U}}_{m,n}^{p,q} + \breve{\mathbf{U}}_{m,n}^{p,q}, \quad m = 1, 2.$$

We choose the first term, $\widetilde{\mathbf{U}}_{m,n}^{p,q}$, to solve (13) with $\mathbf{R}_{m,n}^{p,q}$ identically zero, and the second term, $\breve{\mathbf{U}}_{m,n}^{p,q}$, to solve (13) with $I_{s,n}^{p,q}$, $\widetilde{\mathrm{Q}}_{m,n}^{p,q}$, $\widetilde{J}_n^{p,q}$, and $\mathbf{B}_{m,n}^{p,q}$ all zero. For the sake of simplicity we drop the indices $\{p, q, n\}$, and point out that it is not difficult to see that

$$\widetilde{\mathbf{U}}_m = \mathbf{C}_m e^{i\gamma^{(m)} z} + \mathbf{D}_m e^{-i\gamma^{(m)} z}, \quad m = 1, 2,$$

where the coefficients

$$\mathbf{C}_m = (C_m^x, C_m^y, C_m^z)^T, \quad \mathbf{D}_m = (D_m^x, D_m^y, D_m^z)^T$$

can be explicitly computed from the boundary conditions.

It remains to investigate the equations for $\check{\mathbf{U}}_m$ which can be solved by a High-Order Spectral (HOS) method [71]. As both our Fourier discretization of the lateral variables, $(x, y)$, and the Taylor approximation of the perturbation quantity, $\varepsilon$, are spectrally accurate, it is natural to select a HOS approach to discretize the vertical variable in order to maintain high accuracy. Among HOS approaches, the Legendre–Galerkin methodology [71] appealed to us due to its ease of implementation and stability properties. We have used it in our previous work [36,35] and were impressed with its performance; for this reason we have selected it again in these developments.

However, we have not found the "standard" approaches appearing in the literature useful for our layered media problems and have devised our own "enriched" approach [37,36,35]. To describe this we state that a classic weak formulation of (13) for $\check{\mathbf{U}}_m$ can be specified by: Find $\mathbf{V} \in [H^1([b,a])]^3$ such that

$$(\kappa^2 \mathbf{V}, \mathbf{\Phi}) - (\partial_z \mathbf{V}, \partial_z \mathbf{\Phi}) + (1-\tau) \begin{pmatrix} \left(\partial_z \check{U}_2^x(0) - i\alpha_p \check{U}_2^z(0)\right) \bar{\varphi}^x(0) \\ \left(\partial_z \check{U}_2^y(0) - i\beta_q \check{U}_2^z(0)\right) \bar{\varphi}^y(0) \\ 0 \end{pmatrix}$$
$$= (\mathbf{R}, \mathbf{\Phi}) - i\gamma^{(1)} \check{\mathbf{U}}_1(a) \bar{\mathbf{\Phi}}(a) - i\gamma^{(2)} \check{\mathbf{U}}_2(b) \bar{\mathbf{\Phi}}(b), \quad \forall \mathbf{\Phi} \in [H^1([b,a])]^3,$$

where $I_1 := (0,a)$, $I_2 := (b,0)$,

$$\{\mathbf{V}, \mathbf{R}, \kappa\} = \begin{cases} \{\check{\mathbf{U}}_1, \mathbf{R}_1, \gamma^{(1)}\}, & z \in I_1, \\ \{\check{\mathbf{U}}_2, \mathbf{R}_2, \gamma^{(2)}\}, & z \in I_2. \end{cases}$$

Here the vector pairing on the interval $(a,b)$ is defined by

$$(\mathbf{u}, \mathbf{v}) := \int_a^b \begin{pmatrix} u_1 \bar{v}_1 \\ u_2 \bar{v}_2 \\ u_3 \bar{v}_3 \end{pmatrix} dx,$$

where the overbar denotes complex conjugation.

To construct a Legendre–Galerkin method as in [36,35], we define the finite-dimensional function space $\mathbf{X}_{N_z} \subset [H^1([(b,a)])]^3$ by

$$\mathbf{X}_{N_z} := \{\mathbf{\Phi}_m \in [P_{N_y}(I_m)]^3 \mid \partial_z \mathbf{\Phi}_1(a) - i\gamma^{(1)} \mathbf{\Phi}_1(a) = 0,\ \partial_z \mathbf{\Phi}_2(b) + i\gamma^{(2)} \mathbf{\Phi}_2(b) = 0, m = 1,2\},$$

where $P_{N_z}$ is the space of polynomials of degree less than $N_z$. The Legendre–Galerkin formulation is: Find $\mathbf{U}_{N_z} \in \mathbf{X}_{N_z}$ such that

$$(\kappa^2 \mathbf{U}_{N_z}, \mathbf{\Phi}_{N_z}) - (\partial_z \mathbf{U}_{N_z}, \partial_z \mathbf{\Phi}_{N_z}) + (1-\tau) \begin{pmatrix} \left(\partial_z \check{U}_{2,N_z}^x(0) - i\alpha_p \check{U}_{2,N_z}^z(0)\right) \bar{\varphi}_{N_z}^x(0) \\ \left(\partial_z \check{U}_{2,N_z}^y(0) - i\beta_q \check{U}_{2,N_z}^z(0)\right) \bar{\varphi}_{N_z}^y(0) \\ 0 \end{pmatrix}$$
$$= (\mathcal{I}_{N_z} \mathbf{R}, \mathbf{\Phi}_{N_z}) - i\gamma^{(1)} \check{\mathbf{U}}_{N_z}(a) \bar{\mathbf{\Phi}}_{N_z}(a) - i\gamma^{(2)} \check{\mathbf{U}}_{N_z}(b) \bar{\mathbf{\Phi}}_{N_z}(b), \quad \forall \mathbf{\Phi}_{N_z} \in \mathbf{X}_{N_z},$$

where $\mathcal{I}_{N_z}$ is the projection operator onto $P_{N_z}$. Using integration by parts on each subdomain $I_m$, an equivalent variational formulation is derived: Find $\mathbf{U}_{N_z} \in \mathbf{X}_{N_z}$ such that

$$(\kappa^2 \mathbf{U}_{N_z}, \mathbf{\Phi}_{N_z}) + (\partial_z^2 \mathbf{U}_{N_z}, \mathbf{\Phi}_{N_z}) + \begin{pmatrix} \left(\partial_z \check{U}_{1,N_z}^x(0) - \tau \partial_z \check{U}_{2,N_z}^x(0) - i\alpha_p (\check{U}_{1,N_z}^z(0) - \tau \check{U}_{2,N_z}^z(0))\right) \bar{\varphi}_{N_z}^x(0) \\ \left(\partial_z \check{U}_{1,N_z}^y(0) - \tau \partial_z \check{U}_{2,N_z}^y(0) - i\beta_q (\check{U}_{1,N_z}^z(0) - \tau \check{U}_{2,N_z}^z(0))\right) \bar{\varphi}_{N_z}^y(0) \\ \partial_z \left(\check{U}_{1,N_z}^z(0) - \check{U}_{2,N_z}^z(0)\right) \bar{\varphi}_{N_z}^z(0) \end{pmatrix}$$
$$= (\mathcal{I}_{N_z} \mathbf{R}, \mathbf{\Phi}_{N_z}), \quad \forall \mathbf{\Phi}_{N_z} \in \mathbf{X}_{N_z}.$$

## 5. A Legendre–Galerkin numerical method in enriched spaces

To apply the spectral Legendre–Galerkin approach [70,71] we consider basis functions which are combinations of Legendre polynomials $L_j(z)$. For $z \in I_1$, we define

$$\psi_{1,j}^s(z) := (1+i) L_j\left(\frac{2z-a}{a}\right) + a_{1,j} L_{j+1}\left(\frac{2z-a}{a}\right) + b_{1,j} L_{j+2}\left(\frac{2z-a}{a}\right), \quad j = 1, \ldots, N_z - 2,$$

$s \in \{x, y, z\}$, such that

$$\partial_z \mathbf{\Psi}_{1,j}(a) - i\gamma^{(1)}\mathbf{\Psi}_{1,j}(a) = 0, \quad \mathbf{\Psi}_{1,j}(0) = 0,$$

where

$$\mathbf{\Psi}_{1,j}(z) := (\psi^x_{1,j}, \psi^y_{1,j}, \psi^z_{1,j})^T.$$

Similarly, for $z \in I_2$, we define

$$\psi^s_{2,j}(z) := (1+i)L_j\left(\frac{b-2z}{b}\right) + a_{2,j}L_{j+1}\left(\frac{b-2z}{b}\right) + b_{2,j}L_{j+2}\left(\frac{b-2z}{b}\right), \quad j = 1, \ldots, N_z - 2,$$

$s \in \{x, y, z\}$, such that

$$\partial_z \mathbf{\Psi}_{2,j}(b) + i\gamma^{(2)}\mathbf{\Psi}_{2,j}(b) = 0, \quad \mathbf{\Psi}_{2,j}(0) = 0,$$

where

$$\mathbf{\Psi}_{2,j}(z) = (\psi^x_{2,j}, \psi^y_{2,j}, \psi^z_{2,j})^T.$$

Note that these Legendre–Galerkin basis functions vanish at the transition layer at $z = 0$. For this reason, we introduce additional (enriched) basis functions which have the value $(1+i)$ at $z = 0$:

$$\eta^s(z) := \begin{cases} \eta^s_1(z) = c_1 z + (1+i), & 0 \leqslant z \leqslant a, \\ \eta^s_2(z) = c_2 z + (1+i), & b \leqslant z \leqslant 0, \end{cases}$$

$s \in \{x, y, z\}$, where

$$\partial_z \eta^s_1(a) - i\gamma^{(1)}\eta^s_1(a) = 0, \quad \partial_z \eta^s_2(b) + i\gamma^{(2)}\eta^s_2(b) = 0.$$

We readily find

$$c_1 = \frac{i\gamma^{(1)}}{(1+i) - i\gamma^{(1)}a}, \quad c_2 = \frac{-i\gamma^{(2)}}{(1+i) + i\gamma^{(2)}b}.$$

With these we construct the basis functions defined on $\{b < z < a\}$

$$\tilde{\psi}_j(z) = \begin{cases} \psi^x_{1,j}(z), & 0 < z < a, \\ 0, & b < z < 0, \end{cases} \quad j = 0, \ldots, N_z - 2,$$

and

$$\tilde{\psi}_{N_z+j-1}(z) = \begin{cases} 0, & 0 < z < a, \\ \psi^x_{2,j}(z), & b < z < 0, \end{cases} \quad j = 0, \ldots, N_z - 2,$$

and

$$\tilde{\psi}_{2N_z+j-2}(z) = \begin{cases} \psi^y_{1,j}(z), & 0 < z < a, \\ 0, & b < z < 0, \end{cases} \quad j = 0, \ldots, N_z - 2,$$

and

$$\tilde{\psi}_{3N_z+j-3}(z) = \begin{cases} 0, & 0 < z < a, \\ \psi^y_{2,j}(z), & b < z < 0, \end{cases} \quad j = 0, \ldots, N_z - 2,$$

and

$$\tilde{\psi}_{4N_z+j-4}(z) = \begin{cases} \psi^z_{1,j}(z), & 0 < z < a, \\ 0, & b < z < 0, \end{cases} \quad j = 0, \ldots, N_z - 2,$$

and

$$\tilde{\psi}_{5N_z+j-5}(z) = \begin{cases} 0, & 0 < z < a, \\ \psi^z_{2,j}(z), & b < z < 0, \end{cases} \quad j = 0, \ldots, N_z - 2,$$

and finally,

$$\tilde{\psi}_{6N_z-6} = \eta^x, \quad \tilde{\psi}_{6N_z-5} = \eta^y, \quad \tilde{\psi}_{6N_z-4} = \eta^z.$$

Setting $\bar{N} = 6N_z - 4$, we write our numerical approximation

$$u_{N_z}(z) := \sum_{j=0}^{\bar{N}} \hat{u}_j \tilde{\psi}_j(y),$$

and seek

$$\mathbf{u} = (\hat{u}_0, \hat{u}_1, \ldots, \hat{u}_{\bar{N}})^T,$$

where we are given

$$\mathbf{f} = (\hat{f}_0, \ldots, \hat{f}_{6N_z-7})^T, \quad \hat{f}_j := (\mathcal{I}_N f, \tilde{\psi}_j), \quad j = 0, \ldots, \bar{N}.$$

Here, $f$ stands for the right hand side $\mathbf{R}_m$ in (13).

We define the matrices

$$\begin{aligned}(A_{m,s})_{lj} = &(\partial_y^2 \tilde{\psi}_{(m-1+2(s-1))(N_z-1)+j}, \tilde{\psi}_{(m-1+2(s-1))(N_z-1)+l})_{I_m} \\ &+ (\gamma_{p,q}^{(m)})^2 (\tilde{\psi}_{(m-1+2(s-1))(N_z-1)+j}, \tilde{\psi}_{(m-1+2(s-1))(N_z-1)+l})_{I_m},\end{aligned}$$

where $0 \leqslant l, j \leqslant N_z - 2$, $1 \leqslant m \leqslant 2$, and $1 \leqslant s \leqslant 3$. We set the column vectors

$$\begin{aligned}
a_{12} &= (\partial_z^2 \tilde{\psi}_{6N_z-6}, \tilde{\psi}_j)_{I_1} + (\gamma_{p,q}^{(1)})^2 (\tilde{\psi}_{6N_z-6}, \tilde{\psi}_j)_{I_1}, \\
b_{12} &= (\partial_z^2 \tilde{\psi}_{6N_z-6}, \tilde{\psi}_{N_z+j-1})_{I_2} + (\gamma_{p,q}^{(2)})^2 (\tilde{\psi}_{6N_z-6}, \tilde{\psi}_{N_z+j-1})_{I_2}, \\
c_{13} &= (\partial_z^2 \tilde{\psi}_{6N_z-5}, \tilde{\psi}_{2N_z+j-2})_{I_1} + (\gamma_{p,q}^{(1)})^2 (\tilde{\psi}_{6N_z-5}, \tilde{\psi}_{2N_z+j-2})_{I_1}, \\
d_{13} &= (\partial_z^2 \tilde{\psi}_{6N_z-5}, \tilde{\psi}_{3N_z+j-3})_{I_2} + (\gamma_{p,q}^{(2)})^2 (\tilde{\psi}_{6N_z-5}, \tilde{\psi}_{3N_z+j-3})_{I_2}, \\
e_{14} &= (\partial_z^2 \tilde{\psi}_{6N_z-4}, \tilde{\psi}_{4N_z+j-4})_{I_1} + (\gamma_{p,q}^{(1)})^2 (\tilde{\psi}_{6N_z-4}, \tilde{\psi}_{4N_z+j-4})_{I_1}, \\
f_{14} &= (\partial_z^2 \tilde{\psi}_{6N_z-4}, \tilde{\psi}_{5N_z+j-5})_{I_2} + (\gamma_{p,q}^{(2)})^2 (\tilde{\psi}_{6N_z-4}, \tilde{\psi}_{5N_z+j-5})_{I_2},
\end{aligned}$$

and row vectors

$$\begin{aligned}
a_{21} &= (\partial_z^2 \tilde{\psi}_j, \tilde{\psi}_{6N_z-6})_{I_1} + (\gamma_{p,q}^{(1)})^2 (\tilde{\psi}_j, \tilde{\psi}_{6N_z-6})_{I_1} + \partial_z \tilde{\psi}_j(0) \overline{\tilde{\psi}}_{6N_z-6}(0), \\
b_{21} &= (\partial_z^2 \tilde{\psi}_{N_z+j-1}, \tilde{\psi}_{6N_z-6})_{I_2} + (\gamma_{p,q}^{(2)})^2 (\tilde{\psi}_{N_z+j-1}, \tilde{\psi}_{6N_z-6})_{I_2} - \tau \partial_z \tilde{\psi}_{N_z+j-1}(0) \overline{\tilde{\psi}}_{6N_z-6}(0), \\
c_{31} &= (\partial_z^2 \tilde{\psi}_{2N_z+j-2}, \tilde{\psi}_{6N_z-5})_{I_1} + (\gamma_{p,q}^{(1)})^2 (\tilde{\psi}_{2N_z+j-2}, \tilde{\psi}_{6N_z-5})_{I_1} + \partial_z \tilde{\psi}_{2N_z+j-2}(0) \overline{\tilde{\psi}}_{6N_z-5}(0), \\
d_{31} &= (\partial_z^2 \tilde{\psi}_{3N_z+j-3}, \tilde{\psi}_{6N_z-5})_{I_2} + (\gamma_{p,q}^{(2)})^2 (\tilde{\psi}_{3N_z+j-3}, \tilde{\psi}_{6N_z-5})_{I_2} - \tau \partial_z \tilde{\psi}_{3N_z+j-3}(0) \overline{\tilde{\psi}}_{6N_z-5}(0), \\
e_{41} &= (\partial_z^2 \tilde{\psi}_{4N_z+j-4}, \tilde{\psi}_{6N_z-4})_{I_1} + (\gamma_{p,q}^{(1)})^2 (\tilde{\psi}_{4N_z+j-4}, \tilde{\psi}_{6N_z-4})_{I_1} + \partial_z \tilde{\psi}_{4N_z+j-4}(0) \overline{\tilde{\psi}}_{6N_z-4}(0), \\
f_{41} &= (\partial_z^2 \tilde{\psi}_{5N_z+j-5}, \tilde{\psi}_{6N_z-4})_{I_2} + (\gamma_{p,q}^{(2)})^2 (\tilde{\psi}_{5N_z+j-5}, \tilde{\psi}_{6N_z-4})_{I_2} - \partial_z \tilde{\psi}_{5N_z+j-5}(0) \overline{\tilde{\psi}}_{6N_z-4}(0),
\end{aligned}$$

for $0 \leqslant j \leqslant N_z - 2$. Moreover, we set

$$\begin{aligned}
a_{22} &= (\partial_z^2 \tilde{\psi}_{6N_z-6} + \kappa^2 \tilde{\psi}_{6N_z-6}, \tilde{\psi}_{6N_z-6}) + \partial_z \tilde{\psi}_{6N_z-6}(0^+) \overline{\tilde{\psi}}_{6N_z-6}(0^+) - \tau \partial_z \tilde{\psi}_{6N_z-6}(0^-) \overline{\tilde{\psi}}_{6N_z-6}(0^-), \\
a_{33} &= (\partial_z^2 \tilde{\psi}_{6N_z-5} + \kappa^2 \tilde{\psi}_{6N_z-5}, \tilde{\psi}_{6N_z-5}) + \partial_z \tilde{\psi}_{6N_z-5}(0^+) \overline{\tilde{\psi}}_{6N_z-5}(0^+) - \tau \partial_z \tilde{\psi}_{6N_z-5}(0^-) \overline{\tilde{\psi}}_{6N_z-5}(0^-), \\
a_{44} &= (\partial_z^2 \tilde{\psi}_{6N_z-4} + \kappa^2 \tilde{\psi}_{6N_z-4}, \tilde{\psi}_{6N_z-4}) + \partial_z \tilde{\psi}_{6N_z-4}(0^+) \overline{\tilde{\psi}}_{6N_z-4}(0^+) - \partial_z \tilde{\psi}_{6N_z-4}(0^-) \overline{\tilde{\psi}}_{6N_z-4}(0^-), \\
a_{24} &= -i\alpha(1-\tau) \tilde{\psi}_{6N_z-4}(0) \overline{\tilde{\psi}}_{6N_z-6}(0), \\
a_{34} &= -i\beta(1-\tau) \tilde{\psi}_{6N_z-4}(0) \overline{\tilde{\psi}}_{6N_z-5}(0).
\end{aligned}$$

Here, $\partial_z \tilde{\psi}_n(0^-)$ and $\partial_z \tilde{\psi}_n(0^+)$ stand for the left and right derivatives at 0, respectively. The Legendre–Galerkin scheme demands the $6N_z - 3$ equations:

$$\mathbf{M}\mathbf{u} = \mathbf{f},$$

where $\mathbf{M}$ is a block matrix

$$\mathbf{M} = \begin{pmatrix} A & B \\ C & D \end{pmatrix}.$$

The block matrix $A$ is defined as

$$A = \begin{pmatrix} A_{1,1} & 0 & \dots & & 0 \\ 0 & A_{2,1} & & & \\ & & A_{1,2} & & \vdots \\ \vdots & & & A_{2,2} & \\ & & & & A_{1,3} \quad 0 \\ 0 & & \dots & & 0 \quad A_{2,3} \end{pmatrix},$$

and the block matrices $B$ and $C$ are defined as

$$B = \begin{pmatrix} a_{12} & 0 & 0 \\ b_{12} & 0 & \\ 0 & c_{13} & 0 \\ 0 & d_{13} & 0 \\ 0 & 0 & e_{14} \\ 0 & 0 & f_{14} \end{pmatrix},$$

and

$$C = \begin{pmatrix} (a_{21})^T & (b_{21})^T & 0 & 0 & 0 & 0 \\ 0 & 0 & (c_{31})^T & (d_{31})^T & 0 & 0 \\ 0 & 0 & 0 & 0 & (e_{41})^T & (f_{41})^T \end{pmatrix}.$$

Finally the upper-triangular matrix $D$ is given by

$$D = \begin{pmatrix} a_{22} & 0 & a_{24} \\ 0 & a_{33} & a_{34} \\ 0 & 0 & a_{44} \end{pmatrix}.$$

## 6. Numerical simulations

We now present a variety of numerical experiments utilizing our implementation of the algorithm described above which demonstrate the stability, speed, and accuracy of our methodology. To begin, we demonstrate the performance of our solver for the boundary value problem (13) at the heart of our numerical method using an exact solution. Subsequently we display the fidelity of our *full* scattering solver for (10) using the "energy defect" as an indicator of convergence [65].

### 6.1. Simulations of a boundary value problem

We began by investigating our scheme's numerical approximation of solutions to the reduced problem, (13), which is at the core of our full solver. Utilizing the algorithm proposed in Section 5, we looked for numerical convergence to solutions of the following one-dimensional reduced problem

$$\partial_z^2 \mathbf{u} + \mathbf{k}_u^2 \mathbf{u} = \mathbf{f}_u, \qquad 0 < z < a, \tag{14a}$$
$$\partial_z^2 \mathbf{v} + \mathbf{k}_v^2 \mathbf{v} = \mathbf{f}_v, \qquad b < z < 0, \tag{14b}$$
$$\mathbf{u}(0) = \mathbf{v}(0), \tag{14c}$$
$$\partial_z(u_1(0) - \tau v_1(0)) = i\alpha(u_3(0) - \tau v_3(0)), \tag{14d}$$
$$\partial_z(u_2(0) - \tau v_2(0)) = i\beta(u_3(0) - \tau v_3(0)), \tag{14e}$$
$$\partial_z(u_3(0) - v_3(0)) = 0, \tag{14f}$$
$$\partial_z \mathbf{u}(a) - i\gamma^{(1)}\mathbf{u}(a) = 0, \tag{14g}$$
$$\partial_z \mathbf{v}(b) + i\gamma^{(2)}\mathbf{v}(b) = 0, \tag{14h}$$

where

$$\mathbf{u} = (u_1, u_2, u_3)^T, \quad \mathbf{v} = (v_1, v_2, v_3)^T,$$
$$\mathbf{k}_u^2 = ((k_{u1})^2, (k_{u2})^2, (k_{u3})^2)^T, \quad \mathbf{k}_v^2 = ((k_{v1})^2, (k_{v2})^2, (k_{v3})^2)^T,$$
$$\mathbf{f}_u = (f_{u1}, f_{u2}, f_{u3})^T, \quad \mathbf{f}_v = (f_{v1}, f_{v2}, f_{v3})^T.$$

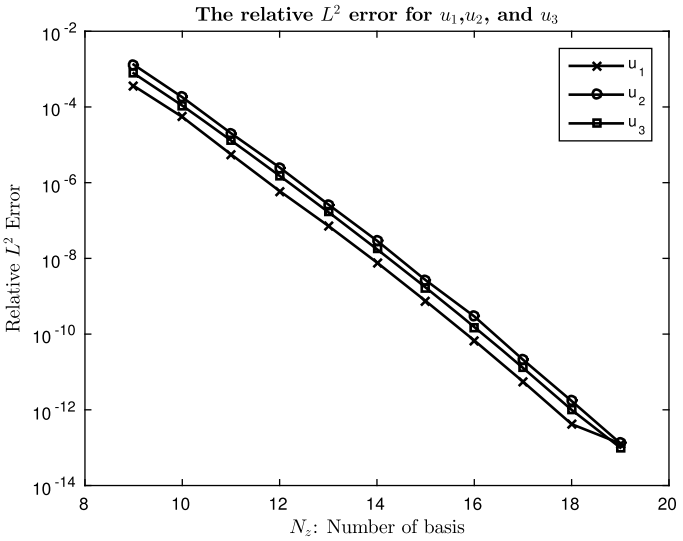


**Fig. 2.** Relative $L^2$ error in $\mathbf{u}$, (16), of our Legendre–Galerkin approximation of (14) in configuration (15) versus number of basis functions $N_z$ on a log-linear scale.

Since the differential operator and boundary conditions in (14) are the same as those in (13), the proposed model provides a good indicator of convergence for our modified Legendre–Galerkin method.

As a test of convergence we considered the following functions and parameters

$$\begin{aligned}
&u_1 = (z-a)^2(z+b)^2, \quad u_2 = \sin(z)(z-a)^2(z+b)^2,\\
&u_3 = \exp(z)(z-a)^2(z+b)^2,\\
&v_1 = (z-a)^2(z+b)^2, \quad v_2 = \sin(z)(z-a)^2(z+b)^2,\\
&v_3 = \exp(z)(z-a)^2(z+b)^2,\\
&a = 5, \quad b = -2, \quad \tau = 1.5, \quad \gamma^{(1)} = 1-i, \quad \gamma^{(2)} = 2+i,\\
&(k_{u1}, k_{u2}, k_{u3}) = (1.25, 2.25, 3.25), \quad (k_{v1}, k_{v2}, k_{v3}) = (2.55, 3.55, 4.55).
\end{aligned} \tag{15}$$

Upon using (14a) and (14b) we can define appropriate $\mathbf{f}_u$ and $\mathbf{f}_v$ so that these represent an exact solution.

To test numerical convergence, we defined the relative $L^2$ error

$$\frac{\|u_{\text{ex}} - u_{N_z}\|_{L^2}}{\|u_{\text{ex}}\|_{L^2}}, \tag{16}$$

where $u_{\text{ex}}$ is the exact solution and $N_z$ is the number of Legendre–Galerkin basis functions. In Figs. 2 and 3 we display the spectral rate of convergence which our Legendre–Galerkin method achieved in this simplified setting. The numerical results illustrate that, given $N_z$ chosen large enough, the proposed modified spectral method can successfully resolve the vector Helmholtz equations with the underlying interfacial boundary conditions.

### *6.2. Simulations of a layered medium: the Maxwell equations*

We also performed numerical experiments of a periodic doubly layered medium whose scattering returns are governed by the full vector Maxwell equations in three dimensions, (10). Unlike the simplified problem in Section 6.1, exact solutions are not available. Hence, we utilized the widely accepted diagnostic of error measurement, the energy defect [65,14]. More precisely, if one considers the Rayleigh expansions in the upper and lower layers

$$\begin{aligned}
\mathbf{H}_1(x,y,z) &= \sum_{p=-\infty}^{\infty}\sum_{q=-\infty}^{\infty} \widehat{\mathbf{H}}_{1,p,q} e^{i(\alpha_p x + \beta_q y + \gamma^{(1)} z)},\\
\mathbf{H}_2(x,y,z) &= \sum_{p=-\infty}^{\infty}\sum_{q=-\infty}^{\infty} \widehat{\mathbf{H}}_{2,p,q} e^{i(\alpha_p x + \beta_q y - \gamma^{(2)} z)},
\end{aligned}$$

quantities of great interest are the *efficiencies*

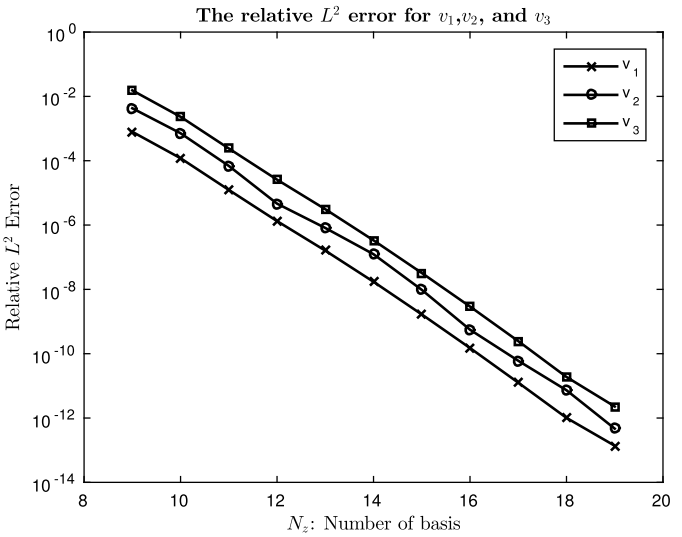


**Fig. 3.** Relative $L^2$ error in $\mathbf{v}$, (16), of our Legendre–Galerkin approximation of (14) in configuration (15) versus number of basis functions $N_z$ on a log-linear scale.

$$e_1^{p,q} := \frac{\gamma_{p,q}^{(1)}}{\gamma} \frac{\left|\widehat{\mathbf{H}}_{1,p,q}\right|^2}{|\mathbf{A}|^2}, \qquad (p,q) \in \mathcal{U}^1,$$

$$e_2^{p,q} := \frac{\gamma_{p,q}^{(2)}}{\gamma} \frac{\left|\widehat{\mathbf{H}}_{2,p,q}\right|^2}{|\mathbf{A}|^2}, \qquad (p,q) \in \mathcal{U}^2,$$

where $\mathbf{A}$ is the amplitude of the incident wave, (1). With this definition in hand, it is clear why these efficiencies are of such interest as they quantify the energy fraction in each mode which propagates away from the grating. If all materials in the structure are lossless ($k_m \in \mathbf{R}$), energy is conserved which is expressed as

$$\sum_{(p,q)\in\mathcal{U}^1} e_1^{p,q} + \tau \sum_{(p,q)\in\mathcal{U}^2} e_2^{p,q} = 1.$$

Hence, we define the "energy defect" as

$$\delta_d := 1 - \sum_{(p,q)\in\mathcal{U}^1} e_1^{p,q} - \tau \sum_{(p,q)\in\mathcal{U}^2} e_2^{p,q},$$

which will be zero for an exact solution [65].

We conducted a sequence of simulations to show the spectral convergence of our proposed Legendre–Galerkin method (in the energy defect measure), and checked the performance of our numerical methods. To begin, we set the following configuration:

$$\begin{aligned} &a = 4, \quad b = -3, \quad (\alpha,\beta,\gamma) = (\sqrt{1/2}, \sqrt{1/3}, 1.2845), \quad d_1 = d_2 = 2\pi, \\ &\mathbf{A} = (\sqrt{3},\sqrt{3},\sqrt{3}), \quad (\gamma^{(1)},\gamma^{(2)}) = (1.2845, 2.0330), \\ &(k_1,k_2) = (1.5758, 2.2285), \quad g(x,y) = \varepsilon\cos(x)\cos(y). \end{aligned} \tag{17}$$

To characterize the performance of our methods we defined the parameters $N$ (perturbation order) and $\{N_x, N_y, N_z\}$ (the number of basis functions in $\{x, y, z\}$ directions). In the first experiment we chose

$$N_x = N_y = 16, \quad N_z = 20, \tag{18}$$

and varied $N$. In Fig. 4 we display the energy defect versus the number of perturbation orders, $N$, retained for the configuration (17) and the parameter choices (18). The figure shows the spectral convergence of the energy defect as the perturbation order is refined. We also see that the energy defect decays more rapidly to machine precision as the value of $\varepsilon$ is reduced.

In Fig. 5 we display results of simulations of configuration (17) with parameter choices

$$N = 12, \quad N_x = N_y = 18, \tag{19}$$

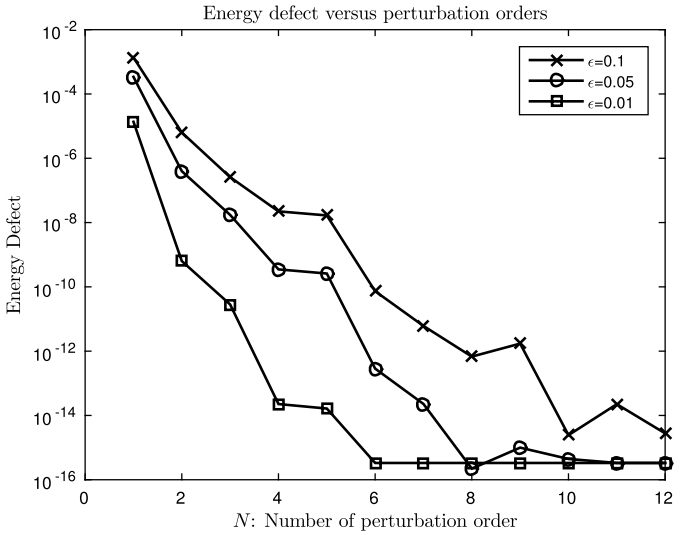


**Fig. 4.** Energy defect versus perturbation order, $N$, for smooth interface configuration (17) and parameter choices (18).

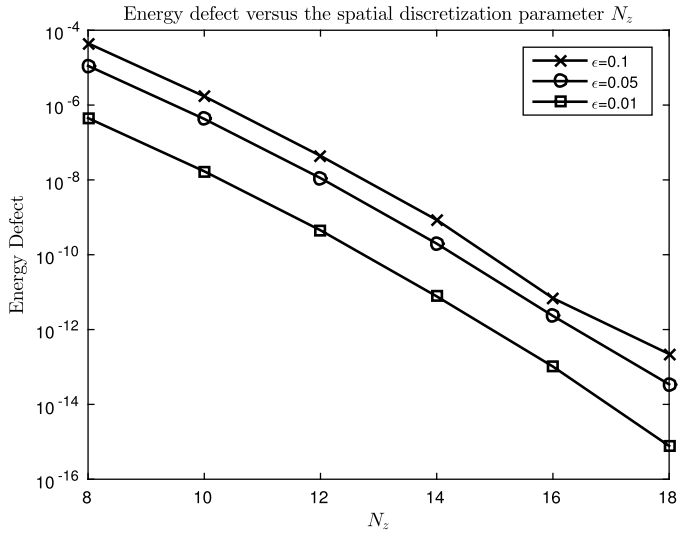


**Fig. 5.** Energy defect versus perturbation order, $N$, for smooth interface configuration (17) and (18).

while varying the vertical discretization parameter, $N_z$. This clearly shows the spectral convergence of the energy defect as this vertical discretization parameter is refined.

In Figs. 6–9 we present the real parts of the scattered solution $H^x$ and $H^z$ from configuration (17) with parameter choices (18) where $\varepsilon = 0.05$. Figs. 6 and 8 present the numerical approximations of $H^x$ and $H^z$ *above* the interface, $\{z = g(x, y)\}$, and Figs. 7 and 9 display the numerical solutions of $H^x$ and $H^z$ *below* the interface, $\{z < g(x, y)\}$.

To continue, we investigate the possibility of using our new algorithm for deformations of *large* size. To examine this, we used the following configuration:

$$\begin{aligned} &a = 2, \quad b = -2, \quad (\alpha, \beta, \gamma) = (\sqrt{1/2}, \sqrt{1/3}, 1.2845), \quad d_1 = d_2 = 2\pi, \\ &\mathbf{A} = (\sqrt{3}, \sqrt{3}, \sqrt{3}), \quad (\gamma^{(1)}, \gamma^{(2)}) = (1.2845, 2.0330), \\ &(k_1, k_2) = (1.5758, 2.2285), \quad g(x, y) = \varepsilon \cos(x) \cos(y), \end{aligned} \tag{20}$$

with numerical parameters $(N_x, N_y, N_z) = (24, 24, 50)$. In Fig. 10, we display numerical simulations with $\varepsilon = 1$. As exhibited in [57,59], simple Taylor summation in perturbation order $N$ does not work well for large or rough deformations. However, if Padé approximation [10] is utilized then outstanding results can be achieved showing that *large* deformations can be readily simulated.

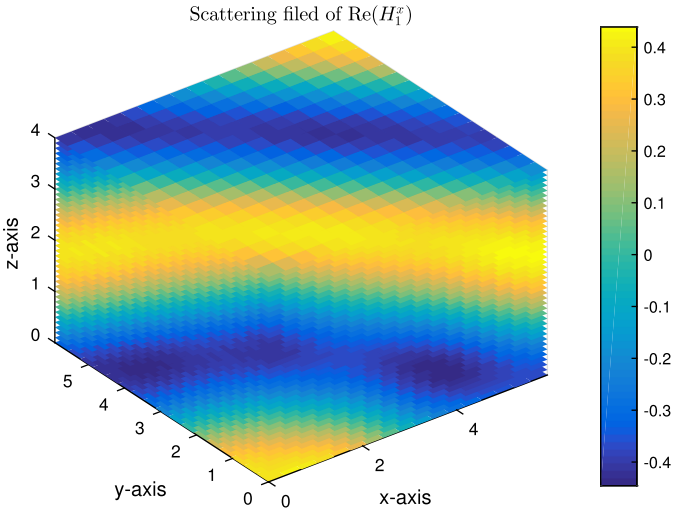


**Fig. 6.** Plot of the real part of the scattered field Re$[H^x]$ above the interface in configuration (17) with parameters (18); for this we chose $\varepsilon = 0.05$ and $N = 12$. (For interpretation of the colors in the figure(s), the reader is referred to the web version of this article.)

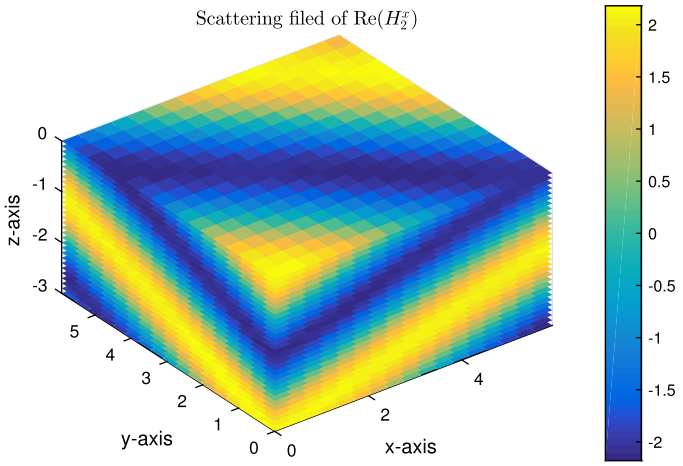


**Fig. 7.** Plot of the real part of the scattered field Re$[H^x]$ below the interface in configuration (17) with parameters (18); for this we chose $\varepsilon = 0.05$ and $N = 12$.

To close, we conducted a numerical simulation with a very *rough* interface defined with the aid of the following "saw-tooth" profile

$$f_L(x) = \begin{cases} -\frac{2}{\pi}x + 1, & 0 \leqslant x \leqslant \pi, \\ \frac{2}{\pi}x - 3, & \pi \leqslant x \leqslant 2\pi, \end{cases}$$

where $f_L$ possesses only Lipschitz regularity [59,60]. For our numerical experiments we used its Fourier series representation

$$f_L(x) = \sum_{k=1}^{\infty} \frac{8}{\pi^2(2k-1)^2} \cos((2k-1)x),$$

which we truncated after wavenumber $P = 20$,

$$f_{L,P}(x) = \sum_{k=1}^{P} \frac{8}{\pi^2(2k-1)^2} \cos((2k-1)x).$$

For these simulations we chose the following parameters:

$$a = 2, \quad b = -2, \quad (\alpha, \beta, \gamma) = (0.2, 0.15, 0.35), \quad d_1 = d_2 = 2\pi,$$

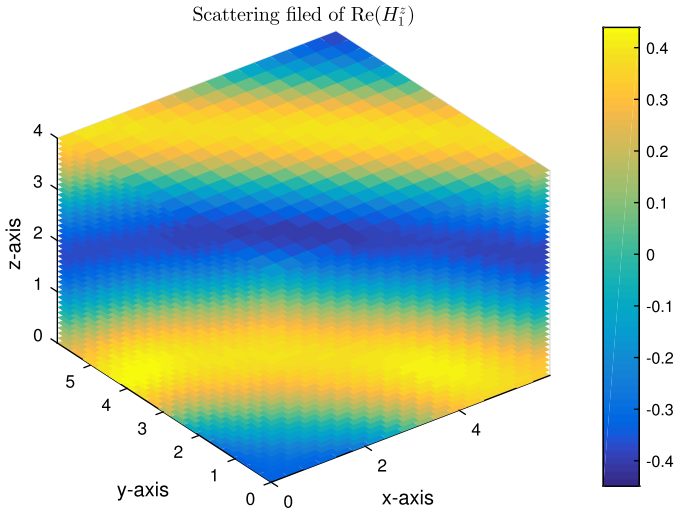


**Fig. 8.** Plot of the real part of the scattered field Re[$H^z$] above the interface in configuration (17) with parameters (18); for this we chose $\varepsilon = 0.05$ and $N = 12$.

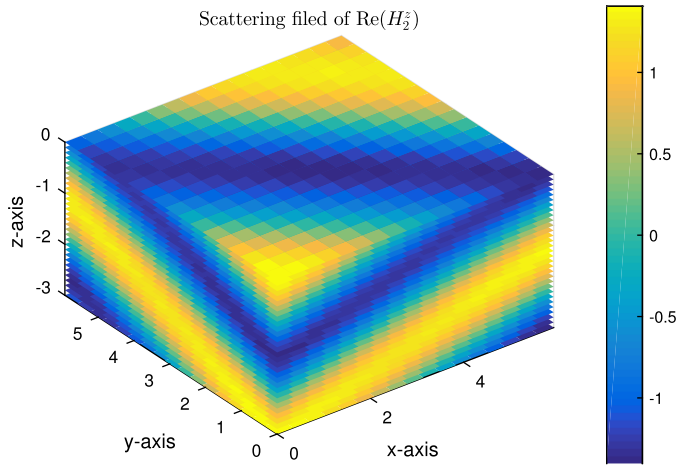


**Fig. 9.** Plot of the real part of the scattered field Re[$H^z$] below the interface in configuration (17) with parameters (18); for this we chose $\varepsilon = 0.05$ and $N = 12$.

$$\mathbf{A} = (\sqrt{3}, \sqrt{3}, \sqrt{3}), \quad (\gamma^{(1)}, \gamma^{(2)}) = (0.35, 0.55453),$$
$$(k_1, k_2) = (0.43012, 0.60828), \quad g(x, y) = \varepsilon f_L(x) \cos(y), \tag{21}$$

with numerical parameters $(N_x, N_y, N_z) = (60, 18, 18)$. In Fig. 11 we display results of our experiment with this rough interface and $\varepsilon = 0.01, 0.05, 0.1$. Evidently, our new method is applicable to configurations with even Lipschitz smoothness, provided that sufficient resolution is utilized.

## 7. Conclusions

We have studied a HOPS algorithm for vector electromagnetic scattering by a periodic, doubly layered medium. In reformulating the time-harmonic Maxwell's equations, a system of vector Helmholtz equations was considered, together with appropriate interfacial boundary conditions. We introduced the TFE algorithm to the resulting problem for the first time, which required that we derive a sequence of one-dimensional, boundary value problems to be solved at each perturbation order in our expansion. Accurate numerical simulations of these TFE recursions were demonstrated with a Legendre–Galerkin method based on a novel weak formulation. These simulations included not only small and smooth interfaces in the periodic structure, but also large and rough ones as well. The numerical simulations showed the spectral convergence which our new algorithm can achieve, and our developments clearly point towards several extensions of great importance. In particular, our approach will be generalized to accommodate surface currents which are one popular approach to modeling two-dimensional materials such as graphene and black phosphorous which are of such great interest to engineers at

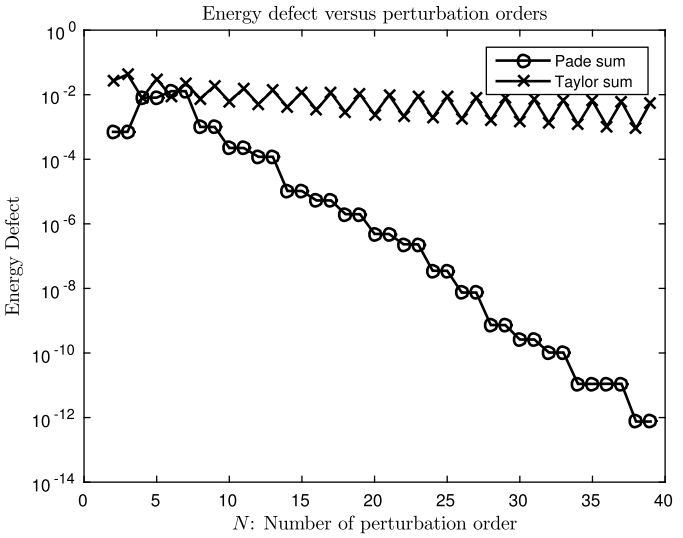


**Fig. 10.** Energy defect versus perturbation order, $N$, for smooth interface configuration with large deformation (20).

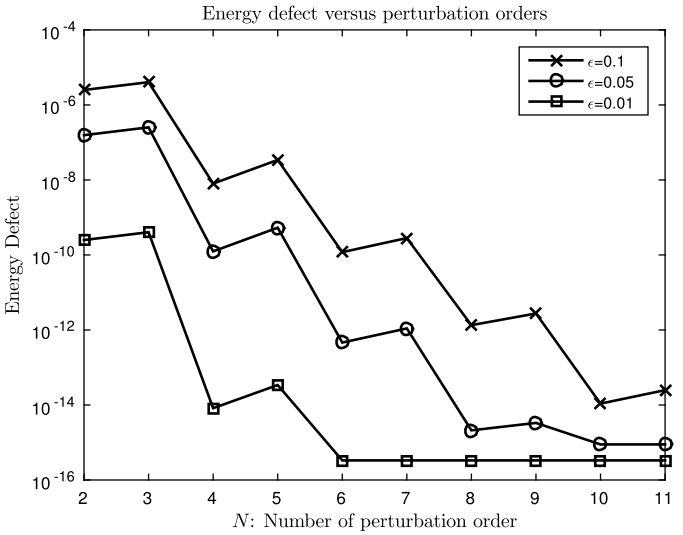


**Fig. 11.** Energy defect versus perturbation order, $N$, for rough interface configuration (21).

the moment [31,8]. This extension will not be straightforward as more subtle boundary conditions between layers must be considered, and hence the algorithmic differences will be significant. In addition, the natural extension to an arbitrary number of layers is clearly in view, and will be considered in a forthcoming article. For a potential roadmap we point the reader to [35] where we achieved this in the simpler context of the Helmholtz equation.

## Acknowledgements

Y.H. gratefully acknowledges support from the Simons Foundation. D.P.N. gratefully acknowledges support from the National Science Foundation through grant No. DMS-1522548. The authors wish to thank Paul Martin and Peter Monk for their advice and guidance.

## Appendix A. Derivation of the transformed equations

In this appendix we provide a full derivation of the transformed equations (11) presented in Section 3.1. By the chain rule, we find

$$\partial_x = \partial_{x'} + (\partial_x z_m)\partial_{z_m}, \quad m = 1, 2,$$

$$\partial_y = \partial_{y'} + (\partial_y z_m)\partial_{z_m}, \quad m = 1, 2,$$
$$\partial_z = (\partial_z z_m)\partial_{z_m}, \quad m = 1, 2.$$

With this we can write

$$(a-g)\nabla_{x,y} = (a-g)\nabla_{x',y'} - (\nabla_{x',y'} g)(a - z_1)\partial_{z_1},$$
$$(a-g)\partial_z = a\partial_{z_1},$$

and

$$(b-g)\nabla_{x,y} = (b-g)\nabla_{x',y'} - (\nabla_{x',y'} g)(z_2 - b)\partial_{z_2},$$
$$(b-g)\partial_z = b\partial_{z_2},$$

where $\nabla_{x,y} = (\partial_x, \partial_y)$ and $\nabla_{x',y'} = (\partial_{x'}, \partial_{y'})$. Defining

$$C_1 = (a-g), \quad D_1^x = -\partial_x g(a - z_1), \quad D_1^y = -\partial_y g(a - z_1), \quad G_1 = a,$$

and

$$C_2 = (g-b), \quad D_2^x = -\partial_x g(b - z_2), \quad D_2^y = -\partial_y g(b - z_2), \quad G_2 = -b,$$

we deduce that

$$C_m\partial_x = C_m\partial_{x'} + D_m^x\partial_{z_m},$$
$$C_m\partial_y = C_m\partial_{y'} + D_m^y\partial_{z_m},$$
$$C_m\partial_z = G_m\partial_{z_m},$$

for $m = 1, 2$.

### A.1. The Helmholtz equation

As in [35], we rewrite the Laplace operator as

$$\begin{aligned} C_m^2\Delta = {} & \nabla_{x',y'}\cdot[C_m^2\nabla_{x',y'}] - (\nabla_{x',y'}C_m)\cdot[C_m\nabla_{x',y'}] + \partial_{z_m}[C_m D_m\cdot\nabla_{x',y'}] \\ & - (\partial_{z_m}D_m)\cdot[C_m\nabla_{x',y'}] + \nabla_{x',y'}\cdot[C_m D_m\partial_{z_m}] - (\nabla_{x',y'}C_m)\cdot[D_m\partial_{z_m}] \\ & + \partial_{z_m}[|D_m|^2\partial_{z_m}] - (\partial_{z_m}D_m)\cdot[D_m\partial_{z_m}] - (\nabla_{x',y'}C_m)\cdot[C_m\nabla_{x',y'}] - (\nabla_{x',y'}C_m)\cdot[D_m\partial_{z_m}] + G_m^2\partial_{z_m}^2, \end{aligned}$$

where $D_m := (D_m^x, D_m^y)$. Then the governing problem becomes

$$\begin{aligned} 0 = {} & C_m^2\Delta_m U_m + C_m^2 k_m^2 U_m \\ = {} & \nabla_{x',y'}\cdot(C_m^2\nabla_{x',y'}U_m) + \partial_{z_m}(C_m D_m\cdot\nabla_{x',y'}U_m) + \nabla_{x',y'}\cdot(C_m D_m\partial_{z_m}U_m) \\ & - (\nabla_{x',y'}C_m)\cdot(D_m\partial_{z_m}U_m) + \partial_{z_m}(|D_m|^2\partial_{z_m}U_m) - (\nabla_{x',y'}C_m)\cdot(C_m\nabla_{x',y'}U_m) + G_m^2\partial_{z_m}^2U_m + C_j^2k_m^2U_m, \end{aligned}$$

where $U_m$ stands for the $x$, $y$, or $z$ components of $\mathbf{U}_m = (U_m^x, U_m^y, U_m^z)^T$. Setting $C_m^2(x) = G_m^2 + F_m(x)$ we deduce that

$$\Delta_m U_m + k_m^2 U_m = \frac{1}{G_m^2}(\partial_{x'}R_m^x + \partial_{y'}R_m^y + \partial_{z_m}R_m^z + R_m^0), \tag{A.1}$$

where

$$R_m^x = -F_m\partial_{x'}U_m - C_m D_m^x\partial_{z_m}U_m, \tag{A.2a}$$
$$R_m^y = -F_m\partial_{y'}U_m - C_m D_m^y\partial_{z_m}U_m, \tag{A.2b}$$
$$R_m^z = -C_m D_m^x\partial_{x'}U_m - (D_m^x)^2\partial_{z_m}U_m - C_m D_m^y\partial_{y'}U_m - (D_m^y)^2\partial_{z_m}U_m, \tag{A.2c}$$
$$R_m^0 = (\partial_{x'}C_m)(D_m^x\partial_{z_m}U_m + C_m\partial_{x'}U_m) + (\partial_{y'}C_m)(D_m^y\partial_{z_m}U_m + C_m\partial_{y'}U_m) - F_m k_m^2 U_m. \tag{A.2d}$$

### A.2. Artificial boundary conditions

For the conditions at the artificial boundaries, $\{z = a\}$ and $\{z = b\}$, of (10), we note that

$$\partial_{z_m} U_m - \frac{C_m}{G_m} T_m[U_m] = 0,$$

and obtain

$$\partial_{z_m} U_m - T_m[U_m] = -\frac{g}{M_m} T_m[U_m], \tag{A.3}$$

for $M_1 = a$ and $M_2 = b$.

### A.3. Interfacial boundary conditions

Regarding the transmission boundary conditions at $z = g(x, y)$ in (10),

$$\mathbf{N} \times (\mathbf{H}_1 - \mathbf{H}_2) = -\mathbf{N} \times \mathbf{H}^{inc},$$

implies that

$$\begin{aligned}
(-\partial_{y'} g)[\![U^z]\!] - [\![U^y]\!] &= \left((\partial_{y'} g) A^z + A^y\right) \varphi, \\
(-\partial_{x'} g)[\![U^z]\!] - [\![U^x]\!] &= \left((\partial_{x'} g) A^z + A^x\right) \varphi.
\end{aligned}$$

Furthermore

$$\mathbf{N} \times (\nabla \times (\mathbf{H}_1 - \tau \mathbf{H}_2)) = -\mathbf{N} \times (\nabla \times \mathbf{H}^{inc}),$$

implies that

$$(-\partial_y g)(\partial_x [\![H^y]\!]_\tau - \partial_y [\![H^x]\!]_\tau) + (\partial_x [\![H^z]\!]_\tau - [\![\partial_z H^x]\!]_\tau) = (\partial_y g)(i\alpha A^y - i\beta A^x)\varphi - (i\alpha A^z + i\gamma A^x)\varphi, \tag{A.4a}$$

and

$$(\partial_x g)(\partial_x [\![H^y]\!]_\tau - \partial_y [\![H^x]\!]_\tau) + (\partial_y [\![H^z]\!]_\tau - [\![\partial_z H^y]\!]_\tau) = -(\partial_x g)(i\alpha A^y - i\beta A^x)\varphi - (i\alpha A^z + i\gamma A^y)\varphi. \tag{A.4b}$$

Noting that, for any scalar function $K$,

$$\begin{aligned}
\partial_x [\![K]\!]_\tau &= \partial_{x'}(K_1 - \tau K_2) + \left(\frac{D_1^x}{C_1}\partial_{z_1} K_1 - \tau \frac{D_2^x}{C_2}\partial_{z_2} K_2\right) \\
&= \partial_{x'} [\![K]\!]_\tau + \left[\!\!\left[\frac{D^x}{C}\partial_z K\right]\!\!\right]_\tau, \\
\partial_y [\![K]\!]_\tau &= \partial_{y'}(K_1 - \tau K_2) + \left(\frac{D_1^y}{C_1}\partial_{z_1} K_1 - \tau \frac{D_2^y}{C_2}\partial_{z_2} K_2\right) \\
&= \partial_{y'} [\![K]\!]_\tau + \left[\!\!\left[\frac{D^y}{C}\partial_z K\right]\!\!\right]_\tau, \\
[\![\partial_z K]\!]_\tau &= \frac{G_1}{C_1}\partial_{z_1} K_1 - \tau \frac{G_2}{C_2}\partial_{z_2} K_2 = \left[\!\!\left[\frac{G}{C}\partial_z K\right]\!\!\right]_\tau,
\end{aligned}$$

we rewrite (A.4) as

$$\begin{aligned}
&(-\partial_{y'} g)\left(\partial_{x'} [\![U^y]\!]_\tau + \left[\!\!\left[\frac{D^x}{C}\partial_z U^y\right]\!\!\right]_\tau - \partial_{y'} [\![U^x]\!]_\tau - \left[\!\!\left[\frac{D^y}{C}\partial_z U^x\right]\!\!\right]_\tau\right) + \left(\partial_{x'} [\![U^z]\!]_\tau + \left[\!\!\left[\frac{D^x}{C}\partial_z U^z\right]\!\!\right]_\tau - \left[\!\!\left[\frac{G}{C}\partial_z U^x\right]\!\!\right]_\tau\right) \\
&\quad = (\partial_y g)(i\alpha A^y - i\beta A^x)\varphi - (i\alpha A^z + i\gamma A^x)\varphi,
\end{aligned} \tag{A.5}$$

and

$$\begin{aligned}
&(\partial_{x'} g)\left(\partial_{x'} [\![U^y]\!]_\tau + \left[\!\!\left[\frac{D^x}{C}\partial_z U^y\right]\!\!\right]_\tau - \partial_{y'} [\![U^x]\!]_\tau - \left[\!\!\left[\frac{D^y}{C}\partial_z U^x\right]\!\!\right]_\tau\right) + \left(\partial_{y'} [\![U^z]\!]_\tau + \left[\!\!\left[\frac{D^y}{C}\partial_z U^z\right]\!\!\right]_\tau - \left[\!\!\left[\frac{G}{C}\partial_z U^y\right]\!\!\right]_\tau\right) \\
&\quad = -(\partial_x g)(i\alpha A^y - i\beta A^x)\varphi - (i\beta A^z + i\gamma A^y)\varphi.
\end{aligned} \tag{A.6}$$

Since $z_1 = z_2 = 0$ at $z = g(x, y)$, we have

$$D_1^x = (-\partial_{x'} g)a, \quad D_1^y = (-\partial_{y'} g)a, \quad D_2^x = (\partial_{x'} g)b, \quad D_2^y = (\partial_{y'} g)b.$$

Hence, we can simplify (A.5) and (A.6) as

$$\partial_{x'} [\![U^z]\!]_\tau - \left[\!\!\left[ \frac{G}{C} \partial_z U^x \right]\!\!\right]_\tau = Q_1,$$
$$\partial_{y'} [\![U^z]\!]_\tau - \left[\!\!\left[ \frac{G}{C} \partial_z U^y \right]\!\!\right]_\tau = Q_2,$$

where

$$Q_1 := (\partial_{y'} g)(i\alpha A^y - i\beta A^x)\varphi - (i\alpha A^z + i\gamma A^x)\varphi - \left[\!\!\left[ \frac{D^x}{C} \partial_z U^z \right]\!\!\right]_\tau + (\partial_{y'} g)\left( \partial_{x'} [\![U^y]\!]_\tau + \left[\!\!\left[ \frac{D^x}{C} \partial_z U^y \right]\!\!\right]_\tau - \partial_{y'} [\![U^x]\!]_\tau - \left[\!\!\left[ \frac{D^y}{C} \partial_z U^x \right]\!\!\right]_\tau \right), \tag{A.7a}$$

$$Q_2 := (-\partial_{x'} g)(i\alpha A^y - i\beta A^x)\varphi - (i\beta A^z + i\gamma A^y)\varphi - \left[\!\!\left[ \frac{D^y}{C} \partial_z U^z \right]\!\!\right]_\tau - (\partial_{x'} g)\left( \partial_{x'} [\![U^y]\!]_\tau + \left[\!\!\left[ \frac{D^x}{C} \partial_z U^y \right]\!\!\right]_\tau - \partial_{y'} [\![U^x]\!]_\tau - \left[\!\!\left[ \frac{D^y}{C} \partial_z U^x \right]\!\!\right]_\tau \right). \tag{A.7b}$$

The divergence free boundary condition

$$C_m \partial_x H_m^x + C_m \partial_y H_m^y + C_m \partial_z H_m^z = 0,$$

transforms to

$$\partial_{x'} U_m^x + \partial_{y'} U_m^y + \frac{G_m}{C_m} \partial_{z_m} U_m^z = -\frac{D_m^x}{C_m} \partial_{z_m} U_m^x - \frac{D_m^y}{C_m} \partial_{z_m} U_m^y.$$

Hence, we deduce that

$$\partial_{x'} U_1^x + \partial_{y'} U_1^y + \frac{a}{a-g} \partial_{z_1} U_1^z = \frac{(\partial_{x'} g)a}{a-g} \partial_{z_1} U_1^x + \frac{(\partial_{y'} g)a}{a-g} \partial_{z_1} U_1^y,$$
$$\partial_{x'} U_2^x + \partial_{y'} U_2^y + \frac{b}{b-g} \partial_{z_2} U_2^z = \frac{(\partial_{x'} g)b}{b-g} \partial_{z_2} U_2^x + \frac{(\partial_{y'} g)b}{b-g} \partial_{z_2} U_2^y.$$

For the other interfacial boundary condition, we simply find that

$$\mathbf{N} \cdot [\![\mathbf{H}]\!] = -\mathbf{N} \cdot \mathbf{H}^{inc}$$

implies that

$$-\partial_{x'} g [\![U^x]\!] - \partial_{y'} g [\![U^y]\!] + [\![U^z]\!] = (\partial_{x'} g)\varphi + (\partial_{y'} g)\varphi - A^z \varphi.$$

Consequently, the transmission boundary conditions in (10) become

$$[\![U^x]\!] = (-\partial_{x'} g)[\![U^z]\!] + ((-\partial_{x'} g)A^z - A^x)\varphi, \tag{A.8a}$$
$$[\![U^y]\!] = (-\partial_{y'} g)[\![U^z]\!] - ((\partial_{y'} g)A^z + A^y)\varphi, \tag{A.8b}$$
$$[\![U^z]\!] = (\partial_{x'} g)[\![U^x]\!] + (\partial_{y'} g)[\![U^y]\!] + ((\partial_{x'} g)A^x + (\partial_{y'} g)A^y - A^z)\varphi, \tag{A.8c}$$
$$\partial_{x'} [\![U^z]\!]_\tau - \left[\!\!\left[ \frac{G}{C} \partial_z U^x \right]\!\!\right]_\tau = Q_1, \tag{A.8d}$$
$$\partial_{y'} [\![U^z]\!]_\tau - \left[\!\!\left[ \frac{G}{C} \partial_z U^y \right]\!\!\right]_\tau = Q_2, \tag{A.8e}$$
$$\partial_{x'} U_1^x + \partial_{y'} U_1^y + \frac{a}{a-g} \partial_{z_1} U_1^z = \frac{(\partial_{x'} g)a}{a-g} \partial_{z_1} U_1^x + \frac{(\partial_{y'} g)a}{a-g} \partial_{z_1} U^y, \tag{A.8f}$$
$$\partial_{x'} U_2^x + \partial_{y'} U_2^y + \frac{b}{b-g} \partial_{z_2} U_2^z = \frac{(\partial_{x'} g)b}{b-g} \partial_{z_2} U_2^x + \frac{(\partial_{y'} g)b}{b-g} \partial_{z_2} U_2^y. \tag{A.8g}$$

### A.4. Boundary perturbation

Considering our specification that $g(x, y) = \varepsilon f(x, y)$, it can be shown that the following expansions converge strongly

$$U_m = \sum_{n=0}^{\infty} U_{m,n}(x, y, z)\varepsilon^n, \quad \text{for } m = 1, 2.$$

In light of this (A.1) becomes

$$\Delta_m U_{m,n} + k_m^2 U_{m,n} = \frac{1}{G_m^2}(\partial_{x'} R^x_{m,n} + \partial_{y'} R^y_{m,n} + \partial_{z_m} R^z_{m,n} + R^0_{m,n}) =: R_{m,n},$$

where

$$\begin{aligned}
R^x_{m,n} &= (2M_m f)\partial_{x'} U_{m,n-1} + M_m \psi_m (\partial_{x'} f)\partial_{z_m} U_{m,n-1} - f^2 \partial_{x'} U_{m,n-2} - f(\partial_{x'} f)\psi_m \partial_{z_m} U_{m,n-2},\\
R^y_{m,n} &= (2M_m f)\partial_{y'} U_{m,n-1} + M_m \psi_m (\partial_{y'} f)\partial_{z_m} U_{m,n-1} - f^2 \partial_{y'} U_{m,n-2} - f(\partial_{y'} f)\psi_m \partial_{z_m} U_{m,n-2},\\
R^z_{m,n} &= M_m(\partial_{'x} f)\psi_m \partial_{x'} U_{m,n-1} + M_m(\partial_{y'} f)\psi_m \partial_{y'} U_{m,n-1} - f(\partial_{x'} f)\psi_m \partial_{x'} U_{m,n-2} - f(\partial_{y'} f)\psi_m \partial_{y'} U_{m,n-2}\\
&\quad - \psi_m^2 \left((\partial_{x'} f)^2 + (\partial_{y'} f)^2\right)\partial_{z_m} U_{m,n-2},\\
R^0_{m,n} &= -M_m(\partial_{x'} f)\partial_{x'} U_{m,n-1} - M_m(\partial_{y'} f)\partial_{y'} U_{m,n-1} + 2M_m f k_m^2 U_{m,n-1} + \left((\partial_{x'} f)^2 + (\partial_{y'} f)^2\right)\psi_m \partial_{z_m} U_{m,n-2}\\
&\quad + (\partial_{x'} f) f \partial_{x'} U_{m,n-2} + (\partial_{y'} f) f \partial_{y'} U_{m,n-2} - f^2 k_m^2 U_{m,n-2}
\end{aligned}$$

for

$$M_1 = a, \quad M_2 = b, \quad \psi_1 = a - z_1, \quad \psi_2 = b - z_2.$$

For the boundary condition (A.3), we write

$$\partial_{z_m} U_{m,n} - T_m[U_{m,n}] = -\frac{f}{M_m} T_m[U_{m,n-1}], \quad \text{for } m = 1, 2.$$

We now consider the transmission boundary conditions (A.8), and, upon setting

$$\varphi_n := e^{i(\alpha x' + \beta y')} \frac{(-i\gamma f)^n}{n!},$$

we write (A.8a) and (A.8b) as

$$\begin{aligned}
[\![U^x_n]\!] &= (-\partial_{x'} f)[\![U^z_{n-1}]\!] - (\partial_{x'} f)A^z \varphi_{n-1} - A^x \varphi_n,\\
[\![U^y_n]\!] &= (-\partial_{y'} f)[\![U^z_{n-1}]\!] - (\partial_{y'} f)A^z \varphi_{n-1} - A^y \varphi_n,
\end{aligned}$$

and (A.8c) as

$$\begin{aligned}
[\![U^z_n]\!] &= (\partial_{x'} f)(U^x_{1,n-1} - U^x_{2,n-1}) + (\partial_{y'} f)(U^y_{1,n-1} - U^y_{2,n-1})\\
&\quad + (\partial_{x'} f)A^x \varphi_{n-1} + (\partial_{y'} f)A^y \varphi_{n-1} - A^z \varphi_n.
\end{aligned}$$

We reformulate (A.8d) and (A.8e) as

$$(\partial_{x'} U^z_{1,n} - \tau \partial_{x'} U^z_{2,n}) - \left(\frac{a}{a-g}\partial_{z_1} U^x_{1,n} - \tau \frac{b}{b-g}\partial_{z_2} U^x_{2,n}\right) = Q_{1,n}, \tag{A.9a}$$

$$(\partial_{y'} U^z_{1,n} - \tau \partial_{y'} U^z_{2,n}) - \left(\frac{a}{a-g}\partial_{z_1} U^y_{1,n} - \tau \frac{b}{b-g}\partial_{z_2} U^y_{2,n}\right) = Q_{2,n}, \tag{A.9b}$$

where

$$\begin{aligned}
Q_{1,n} &= (\partial_{y'} f)(i\alpha A^y - i\beta A^x)\varphi_{n-1} - (i\alpha A^x + i\gamma A^x)\varphi_n + \left(\frac{a\partial_{x'} f}{a-g}\partial_{z_1} U^z_{1,n-1} + \tau \frac{b\partial_{x'} f}{g-b}\partial_{z_2} U^z_{2,n-1}\right)\\
&\quad + (\partial_{y'} f)\left(\frac{(-\partial_{x'} f)a}{a-g}\partial_{z_1} U^y_{1,n-2} - \tau \frac{(\partial_{x'} f)b}{g-b}\partial_{z_2} U^y_{2,n-2} - \frac{(-\partial_{y'} f)a}{a-g}\partial_{z_1} U^x_{1,n-2} + \tau \frac{(\partial_{y'} b)b}{g-b}\partial_{z_2} U^x_{2,n-2}\right)\\
&\quad + (\partial_{y'} f)\left(\partial_{x'} U^y_{1,n-1} - \tau \partial_{x'} U^y_{2,n-1} - \partial_{y'} U^x_{1,n-1} + \tau \partial_{y'} U^x_{2,n-1}\right),
\end{aligned}$$

and

$$
\begin{aligned}
Q_{2,n} = {} & (-\partial_{x'} f)(i\alpha A^y - i\beta A^x)\varphi_{n-1} - (i\beta A^z + i\gamma A^y)\varphi_n - \left( \frac{(-\partial_{y'} f)a}{a-g}\partial_{z_1} U^z_{1,n-1} - \tau \frac{(\partial_{y'} f)b}{g-b}\partial_{z_2} U^z_{2,n-1} \right) \\
& - (\partial_{x'} f)\left( \frac{(-\partial_{x'} f)a}{a-g}\partial_{z_1} U^y_{1,n-2} - \tau \frac{(\partial_{x'} f)b}{g-b}\partial_{z_2} U^y_{2,n-2} - \frac{(-\partial_{y'} f)a}{a-g}\partial_{z_1} U^x_{1,n-2} + \tau \frac{(\partial_{y'} b)b}{g-b}\partial_{z_2} U^x_{2,n-2} \right) \\
& - (\partial_{x'} f)\left( \partial_{x'} U^y_{1,n-1} - \tau \partial_{x'} U^y_{2,n-1} - \partial_{y'} U^x_{1,n-1} + \tau \partial_{y'} U^x_{2,n-1} \right).
\end{aligned}
$$

Multiplying (A.9) by $(a-g)(b-g)$ we rearrange these equations

$$
\begin{aligned}
&(\partial_{x'} U^z_{1,n} - \tau \partial_{x'} U^z_{2,n}) - (\partial_{z_1} U^x_{1,n} - \tau \partial_{z_2} U^x_{2,n}) = \widetilde{Q}_{1,n}, \\
&(\partial_{y'} U^z_{1,n} - \tau \partial_{y'} U^z_{2,n}) - (\partial_{z_1} U^y_{1,n} - \tau \partial_{z_2} U^y_{2,n}) = \widetilde{Q}_{2,n},
\end{aligned}
$$

where

$$
\begin{aligned}
\widetilde{Q}_{1,n} = {} & \frac{1}{ab}\big( f(a+b)(\partial_{x'} U^z_{1,n-1} - \tau \partial_{x'} U^z_{2,n-1}) - af\partial_{z_1} U^x_{1,n-1} + \tau bf \partial_{z_2} U^x_{2,n-1} \\
& - f^2 \partial_{x'} U^z_{1,n-2} + \tau f^2 \partial_{x'} U^z_{2,n-2} + ab Q_{1,n} - (a+b) f Q_{1,n-1} + f^2 Q_{1,n-2} \big),
\end{aligned}
$$

and

$$
\begin{aligned}
\widetilde{Q}_{2,n} = {} & \frac{1}{ab}\big( f(a+b)(\partial_{y'} U^z_{1,n-1} - \tau \partial_{y'} U^z_{2,n-1}) - af\partial_{z_1} U^y_{1,n-1} + \tau bf \partial_{z_2} U^y_{2,n-1} \\
& - f^2 \partial_{y'} U^z_{1,n-2} + \tau f^2 \partial_{y'} U^z_{2,n-2} + ab Q_{2,n} - (a+b) f Q_{2,n-1} + f^2 Q_{2,n-2} \big).
\end{aligned}
$$

If we multiply (A.8f) by $(a-g)/a$ and (A.8g) by $(b-g)/b$, respectively, and simplify the divergence free conditions we find

$$
\begin{aligned}
&\partial_{x'} U^x_{1,n} + \partial_{y'} U^y_{1,n} + \partial_{z_1} U^z_{1,n} \\
&\quad = (\partial_{x'} f)\partial_{z_1} U^x_{1,n-1} + (\partial_{y'} f)\partial_{z_1} U^y_{1,n-1} + \frac{f}{a}\partial_{x'} U^x_{1,n-1} + \frac{f}{a}\partial_{y'} U^y_{1,n-1},
\end{aligned}
$$

and

$$
\begin{aligned}
&\partial_{x'} U^x_{2,n} + \partial_{y'} U^y_{2,n} + \partial_{z_2} U^z_{2,n} \\
&\quad = (\partial_{x'} f)\partial_{z_2} U^x_{2,n-1} + (\partial_{y'} f)\partial_{z_2} U^y_{2,n-1} + \frac{f}{b}\partial_{x'} U^x_{2,n-1} + \frac{f}{b}\partial_{y'} U^y_{2,n-1}.
\end{aligned}
$$

By subtracting these equations, we complete the interfacial boundary condition

$$
\partial_{x'}(U^x_{1,n} - U^x_{2,n}) + \partial_{y'}(U^y_{1,n} - U^y_{2,n}) + (\partial_{z_1} U^z_{1,n} - \partial_{z_2} U^z_{2,n}) = \tilde{J}_n,
$$

where

$$
\begin{aligned}
\tilde{J}_n := {} & (\partial_{x'} f)(\partial_{z_1} U^x_{1,n-1} - \partial_{z_2} U^x_{2,n-1}) + (\partial_{y'} f)(\partial_{z_1} U^y_{1,n-1} - \partial_{z_2} U^y_{2,n-1}) \\
& + \left( \frac{f}{a}\partial_{x'} U^x_{1,n-1} - \frac{f}{b}\partial_{x'} U^x_{2,n-1} \right) + \left( \frac{f}{a}\partial_{y'} U^y_{1,n-1} - \frac{f}{b}\partial_{y'} U^y_{2,n-1} \right).
\end{aligned}
$$

In conclusion, we arrive at the following equations:

$$
\begin{aligned}
&\Delta_1 \mathbf{U}_{1,n} + k_1^2 \mathbf{U}_{1,n} = \mathbf{R}_{1,n}, && \text{in } 0 < z < a, && \text{(A.10a)} \\
&\Delta_2 \mathbf{U}_{2,n} + k_2^2 \mathbf{U}_{2,n} = \mathbf{R}_{2,n}, && \text{in } b < z < 0, && \text{(A.10b)} \\
&[\![ U^x_n ]\!] = I_{1,n}, && \text{at } z_1 = z_2 = 0, && \text{(A.10c)} \\
&[\![ U^y_n ]\!] = I_{2,n}, && \text{at } z_1 = z_2 = 0, && \text{(A.10d)} \\
&[\![ U^z_n ]\!] = I_{3,n}, && \text{at } z_1 = z_2 = 0, && \text{(A.10e)} \\
&[\![ \partial_{x'} U^z_n ]\!]_\tau [\![ \partial_z U^x_n ]\!]_\tau = \widetilde{Q}_1, && \text{at } z_1 = z_2 = 0, && \text{(A.10f)} \\
&[\![ \partial_{y'} U^z_n ]\!]_\tau [\![ \partial_z U^y_n ]\!]_\tau = \widetilde{Q}_2, && \text{at } z_1 = z_2 = 0, && \text{(A.10g)} \\
&[\![ \partial_{x'} U^x_n ]\!] + [\![ \partial_{y'} U^y_n ]\!] + [\![ \partial_z U^z_n ]\!] = \tilde{J}_n, && \text{at } z_1 = z_2 = 0, && \text{(A.10h)} \\
&\partial_{z_1} \mathbf{U}_{1,n} - T_1[\mathbf{U}_{1,n}] = \mathbf{B}_{1,n}, && \text{at } z_1 = a, && \text{(A.10i)} \\
&\partial_{z_2} \mathbf{U}_{2,n} - T_2[\mathbf{U}_{2,n}] = \mathbf{B}_{2,n}, && \text{at } z_2 = b, && \text{(A.10j)}
\end{aligned}
$$

where

$$
\begin{aligned}
I_{1,n} &:= (-\partial_{x'} f)(U^z_{1,n-1} - U^z_{2,n-1}) - (\partial_{x'} f) A^z \varphi_{n-1} - A^x \varphi_n, \\
I_{2,n} &:= (-\partial_{y'} f)(U^z_{1,n-1} - U^z_{2,n-1}) - (\partial_{y'} f) A^z \varphi_{n-1} - A^y \varphi_n, \\
I_{3,n} &:= (\partial_{x'} f)(U^x_{1,n-1} - U^x_{2,n-1}) + (\partial_{y'} f)(U^y_{1,n-1} - U^y_{2,n-1}) \\
&\quad + (\partial_{x'} f) A^x \varphi_{n-1} + (\partial_{y'} f) A^y \varphi_{n-1} - A^z \varphi_n
\end{aligned}
$$

and

$$
\begin{aligned}
\mathbf{B}_{1,n} &= -\frac{f}{a} T_1[\mathbf{U}_{1,n-1}], \\
\mathbf{B}_{2,n} &= -\frac{f}{b} T_2[\mathbf{U}_{2,n-1}].
\end{aligned}
$$

## References


[1] H.A. Atwater, A. Polman, Plasmonics for improved photovoltaic devices, Nat. Mater. 9 (2010) 205.
[2] Tilo Arens, Scattering by Biperiodic Layered Media: The Integral Equation Approach, Habilitationsschrift, Karlsruhe Institute of Technology, 2009.
[3] O. Bruno, B. Delourme, Rapidly convergent two-dimensional quasi-periodic Green function throughout the spectrum-including Wood anomalies, J. Comput. Phys. 262 (2014) 262–290.
[4] Jean-Pierre Bérenger, A perfectly matched layer for the absorption of electromagnetic waves, J. Comput. Phys. 114 (2) (1994) 185–200.
[5] Jean-Pierre Bérenger, Evanescent waves in PML's: origin of the numerical reflection in wave-structure interaction problems, IEEE Trans. Antennas Propag. 47 (10) (1999) 1497–1503.
[6] Gang Bao, Avner Friedman, Inverse problems for scattering by periodic structures, Arch. Ration. Mech. Anal. 132 (1) (1995) 49–72.
[7] Oscar P. Bruno, Agustin G. Fernandez-Lado, Rapidly convergent quasi-periodic Green functions for scattering by arrays of cylinders-including Wood anomalies, Proc. R. Soc. A, Math. Phys. Eng. Sci. 473 (2199) (2017) 20160802, 23.
[8] Y. Bludov, A. Ferreira, N. Peres, M. Vasilevskiy, A primer on surface plasmon–polaritons in graphene, Int. J. Mod. Phys. B 27 (2013) 1341001.
[9] A. Barnett, L. Greengard, A new integral representation for quasi-periodic scattering problems in two dimensions, BIT Numer. Math. 51 (2011) 67–90.
[10] George A. Baker Jr., Peter Graves-Morris, Padé Approximants, second edition, Cambridge University Press, Cambridge, 1996.
[11] Oscar P. Bruno, Mark Lyon, Carlos Pérez-Arancibia, Catalin Turc, Windowed Green function method for layered-media scattering, SIAM J. Appl. Math. 76 (5) (2016) 1871–1898.
[12] T. Binford, D.P. Nicholls, N. Nigam, T. Warburton, Exact non-reflecting boundary conditions on general domains and hp-finite elements, J. Sci. Comput. 39 (2) (2009) 265–292.
[13] O.P. Bruno, C. Pérez-Arancibia, Windowed Green function method for the Helmholtz equation in the presence of multiply layered media, Proc. R. Soc. A, Math. Phys. Eng. Sci. 473 (2202) (2017) 20170161, 20.
[14] O. Bruno, F. Reitich, Numerical solution of diffraction problems: a method of variation of boundaries, J. Opt. Soc. Am. A 10 (6) (1993) 1168–1175.
[15] O. Bruno, F. Reitich, Numerical solution of diffraction problems: a method of variation of boundaries, II: finitely conducting gratings, Padé approximants, and singularities, J. Opt. Soc. Am. A 10 (11) (1993) 2307–2316.
[16] O. Bruno, F. Reitich, Numerical solution of diffraction problems: a method of variation of boundaries, III: doubly periodic gratings, J. Opt. Soc. Am. A 10 (12) (1993) 2551–2562.
[17] Oscar P. Bruno, Fernando Reitich, Approximation of analytic functions: a method of enhanced convergence, Math. Comput. 63 (207) (1994) 195–213.
[18] Oscar P. Bruno, Fernando Reitich, Calculation of electromagnetic scattering via boundary variations and analytic continuation, Appl. Comput. Electromagn. Soc. J. 11 (1) (1996) 17–31.
[19] Oscar P. Bruno, Fernando Reitich, Boundary-variation solutions for bounded-obstacle scattering problems in three dimensions, J. Acoust. Soc. Am. 104 (5) (1998) 2579–2583.
[20] Oscar P. Bruno, Fernando Reitich, High-order boundary perturbation methods, in: Mathematical Modeling in Optical Science, in: Frontiers in Applied Mathematics Series, vol. 22, SIAM, Philadelphia, PA, 2001, pp. 71–109.
[21] Oscar P. Bruno, Stephen P. Shipman, Catalin Turc, Stephanos Venakides, Superalgebraically convergent smoothly windowed lattice sums for doubly periodic Green functions in three-dimensional space, Proc. R. Soc. A, Math. Phys. Eng. Sci. 472 (2191) (2016) 20160255, 19.
[22] Min Hyun Cho, Alex Barnett, Robust fast direct integral equation solver for quasi-periodic scattering problems with a large number of layers, Opt. Express 23 (2) (2015) 1775–1799.
[23] Xinfu Chen, Avner Friedman, Maxwell's equations in a periodic structure, Trans. Am. Math. Soc. 323 (2) (1991) 465–507.
[24] David Colton, Rainer Kress, Inverse Acoustic and Electromagnetic Scattering Theory, third edition, Applied Mathematical Sciences, vol. 93, Springer, New York, 2013.
[25] J. Chandezon, D. Maystre, G. Raoult, A new theoretical method for diffraction gratings and its numerical application, J. Opt. 11 (7) (1980) 235–241.
[26] David Dobson, Avner Friedman, The time-harmonic Maxwell equations in a doubly periodic structure, J. Math. Anal. Appl. 166 (2) (1992) 507–528.
[27] M.O. Deville, P.F. Fischer, E.H. Mund, High-Order Methods for Incompressible Fluid Flow, Cambridge Monographs on Applied and Computational Mathematics, vol. 9, Cambridge University Press, Cambridge, 2002.
[28] T.W. Ebbesen, H.J. Lezec, H.F. Ghaemi, T. Thio, P.A. Wolff, Extraordinary optical transmission through sub-wavelength hole arrays, Nature 391 (6668) (1998) 667–669.
[29] Q. Fang, D.P. Nicholls, J. Shen, A stable, high-order method for three-dimensional bounded-obstacle scattering, J. Comput. Phys. 224 (2) (2007) 1145–1169.
[30] D. Givoli, Recent advances in the DtN FE method, Arch. Comput. Methods Eng. 6 (2) (1999) 71–116.
[31] A. Geim, K. Novoselov, The rise of graphene, Nat. Mater. 6 (2007) 183–191.
[32] D. Gottlieb, S.A. Orszag, Numerical analysis of spectral methods: theory and applications, in: CBMS–NSF Regional Conference Series in Applied Mathematics, vol. 26, Society for Industrial and Applied Mathematics, Philadelphia, Pa, 1977.
[33] L. Greengard, V. Rokhlin, A fast algorithm for particle simulations, J. Comput. Phys. 73 (2) (1987) 325–348.
[34] B. Hu, D.P. Nicholls, The domain of analyticity of Dirichlet–Neumann operators, Proc. R. Soc. Edinb., Sect. A, Math. 140 (2) (2010) 367–389.
[35] Y. Hong, D.P. Nicholls, A high-order perturbation of surfaces method for scattering of linear waves by periodic multiply layered gratings in two and three dimensions, J. Comput. Phys. 345 (2017) 162–188.

[36] Y. Hong, D.P. Nicholls, A stable high-order perturbation of surfaces method for numerical simulation of diffraction problems in triply layered media, J. Comput. Phys. 330 (2017) 1043–1068.
[37] Y. He, D.P. Nicholls, J. Shen, An efficient and stable spectral method for electromagnetic scattering from a layered periodic structure, J. Comput. Phys. 231 (8) (2012) 3007–3022.
[38] J. Homola, Surface plasmon resonance sensors for detection of chemical and biological species, Chem. Rev. 108 (2) (2008) 462–493.
[39] Hou De Han, Xiao Nan Wu, Approximation of infinite boundary condition and its application to finite element methods, J. Comput. Math. 3 (2) (1985) 179–192.
[40] Jan S. Hesthaven, Tim Warburton, Nodal Discontinuous Galerkin Methods: Algorithms, Analysis, and Applications, in: Texts in Applied Mathematics, vol. 54, Springer, New York, 2008.
[41] Claes Johnson, J. -Claude Nédélec, On the coupling of boundary integral and finite element methods, Math. Comput. 35 (152) (1980) 1063–1079.
[42] Claes Johnson, Numerical Solution of Partial Differential Equations by the Finite Element Method, Cambridge University Press, Cambridge, 1987.
[43] Bo-Nan Jiang, Jie Wu, L.A. Povinelli, The origin of spurious solutions in computational electromagnetics, J. Comput. Phys. 125 (1) (1996) 104–123.
[44] Joseph B. Keller, Dan Givoli, Exact nonreflecting boundary conditions, J. Comput. Phys. 82 (1) (1989) 172–192.
[45] Urve Kangro, Roy Nicolaides, Divergence boundary conditions for vector Helmholtz equations with divergence constraints, Modél. Math. Anal. Numér. 33 (3) (1999) 479–492.
[46] Randall J. LeVeque, Finite Difference Methods for Ordinary and Partial Differential Equations: Steady-State and Time-Dependent Problems, Society for Industrial and Applied Mathematics (SIAM), Philadelphia, PA, 2007.
[47] N.C. Lindquist, T.W. Johnson, J. Jose, L.M. Otto, S.-H. Oh, Ultrasmooth metallic films with buried nanostructures for backside reflection-mode plasmonic biosensing, Ann. Phys. 524 (2012) 687–696.
[48] D. Michael Milder, An improved formalism for rough-surface scattering of acoustic and electromagnetic waves, in: Proceedings of SPIE – The International Society for Optical Engineering, San Diego, 1991, vol. 1558, Int. Soc. for Optical Engineering, Bellingham, WA, 1991, pp. 213–221.
[49] D. Michael Milder, An improved formalism for wave scattering from rough surfaces, J. Acoust. Soc. Am. 89 (2) (1991) 529–541.
[50] M. Moskovits, Surface-enhanced spectroscopy, Rev. Mod. Phys. 57 (3) (1985) 783–826.
[51] D. Michael Milder, H. Thomas Sharp, Efficient computation of rough surface scattering, in: Mathematical and Numerical Aspects of Wave Propagation Phenomena, Strasbourg, 1991, SIAM, Philadelphia, PA, 1991, pp. 314–322.
[52] D. Michael Milder, H. Thomas Sharp, An improved formalism for rough surface scattering, II: numerical trials in three dimensions, J. Acoust. Soc. Am. 91 (5) (1992) 2620–2626.
[53] D.P. Nicholls, A method of field expansions for vector electromagnetic scattering by layered periodic crossed gratings, J. Opt. Soc. Am. A 32 (5) (2015) 701–709.
[54] D.P. Nicholls, N. Nigam, Exact non-reflecting boundary conditions on general domains, J. Comput. Phys. 194 (1) (2004) 278–303.
[55] D.P. Nicholls, S.-H. Oh, T.W. Johnson, F. Reitich, Launching surface plasmon waves via vanishingly small periodic gratings, J. Opt. Soc. Am. A 33 (3) (2016) 276–285.
[56] D.P. Nicholls, F. Reitich, A new approach to analyticity of Dirichlet–Neumann operators, Proc. R. Soc. Edinb., Sect. A, Math. 131 (6) (2001) 1411–1433.
[57] D.P. Nicholls, F. Reitich, Stability of high-order perturbative methods for the computation of Dirichlet–Neumann operators, J. Comput. Phys. 170 (1) (2001) 276–298.
[58] D.P. Nicholls, F. Reitich, Analytic continuation of Dirichlet–Neumann operators, Numer. Math. 94 (1) (2003) 107–146.
[59] D.P. Nicholls, F. Reitich, Shape deformations in rough surface scattering: cancellations, conditioning, and convergence, J. Opt. Soc. Am. A 21 (4) (2004) 590–605.
[60] D.P. Nicholls, F. Reitich, Shape deformations in rough surface scattering: improved algorithms, J. Opt. Soc. Am. A 21 (4) (2004) 606–621.
[61] D.P. Nicholls, F. Reitich, T.W. Johnson, S.-H. Oh, Fast high-order perturbation of surfaces (HOPS) methods for simulation of multi-layer plasmonic devices and metamaterials, J. Opt. Soc. Am. A 31 (8) (2014) 1820–1831.
[62] D.P. Nicholls, J. Shen, A stable, high-order method for two-dimensional bounded-obstacle scattering, SIAM J. Sci. Comput. 28 (4) (2006) 1398–1419.
[63] D.P. Nicholls, J. Shen, A rigorous numerical analysis of the transformed field expansion method, SIAM J. Numer. Anal. 47 (4) (2009) 2708–2734.
[64] D.P. Nicholls, V. Tammali, A high-order perturbation of surfaces (HOPS) approach to Fokas integral equations: vector electromagnetic scattering by periodic crossed gratings, Appl. Numer. Methods 101 (2016) 1–17.
[65] R. Petit (Ed.), Electromagnetic Theory of Gratings, Springer-Verlag, Berlin, 1980.
[66] N.A. Phillips, A coordinate system having some special advantages for numerical forecasting, J. Atmos. Sci. 14 (2) (1957) 184–185.
[67] Rayleigh Lord, On the dynamical theory of gratings, Proc. R. Soc. Lond. Ser. A 79 (1907) 399–416.
[68] S.O. Rice, Reflection of electromagnetic waves from slightly rough surfaces, Commun. Pure Appl. Math. 4 (1951) 351–378.
[69] F. Reitich, K. Tamma, State-of-the-art, trends, and directions in computational electromagnetics, CMES Comput. Model. Eng. Sci. 5 (4) (2004) 287–294.
[70] Jie Shen, Efficient spectral-Galerkin method, I: direct solvers of second- and fourth-order equations using Legendre polynomials, SIAM J. Sci. Comput. 15 (6) (1994) 1489–1505.
[71] Jie Shen, Tao Tang, Li-Lian Wang, Spectral Methods: Algorithms, Analysis and Applications, in: Springer Series in Computational Mathematics, vol. 41, Springer, Heidelberg, 2011.
[72] H. Xu, E. Bjerneld, M. Käll, L. Börjesson, Spectroscopy of single hemoglobin molecules by surface enhanced Raman scattering, Phys. Rev. Lett. 83 (1999) 4357–4360.